D A T A P R O B L E M S

IN

MEDIUM RANGE WEATHER FORECASTING

B Y

P. M O R E L

LABORATOIRE DE METEOROLOGIE DYNAMIQUE

DU C.N.R.S.

1. The W.W.W. Surface and Upper-Air Network

It does not befit well this speaker to describe the World Weather Watch Global Observing System of surface and upper air stations to practising meteorologists who attend this series of lectures. He will therefore attempt to be very brief on the general plans and implementation of this remarkable system which are excellently described in W.M.O. publications (1), and he will dwell more on some possibly lesser known and basic characteristics of meteorological measurements.

In the first place we should ask ourselves the very basic question of all experimental sciences: what is it that we want to observe, what are its characteristic space and time scales and how accurately do we need to measure it? As a matter of fact this cartesian approach was not even considered up to the recent years. For so great is the complexity of atmospheric processes and so scarce were our observations that the meteorologists could only cry for more stations and more data. And to some extent, the current plans for the implementation of the World Weather Watch still reflect this general feeling for an everlasting need to maintain all available observing possibilities, acquire as many new stations and communicate as many pieces of information as one can possibly contemplate. Is this justified and how far are we from achieving a "complete" coverage of the planetary atmosphere?

In this context it may be illuminating to consider the kinematics of the global atmosphere as illustrated by a short sequence of the EOLE movie, showing the airflow at about 200mb over the Southern Hemisphere, as indicated by the animated trajectories of nearly 200 constant level balloons floating freely in the lower stratosphere. The interesting features to note are (i) the time scale of the significant weather systems which develop in a matter of one to two days and last less than a week; (ii) the spatial scale of these weather systems which rarely exceeds a characteristic length of 1000 km. We may conclude then from this brief overview and from the results of many a learned study of atmosphere dynamics that characterizing the state of motions of the planetary atmosphere and the significant patterns of the general circulation requires that observations be everywhere dense with sampling intervals of 0.5 to one day in the time domain and 500-700 km in the spatial domain. How well does the current surface and upper air network fare in regard of these requirements?

Global coverage and sampling density

Figure 1 is a map of upper air stations in the Northern Hemisphere extratropics. It will be noticed that upper air observations are indeed quite appropriately dense over all northern continental areas. Note that the blank over China does not reflect upon the quality of the Chinese meteorological network but only the fact that China was not a member of W.M.O. at the time this map was drafted. One will notice also that upper air, and to a lesser extent surface observations, are far

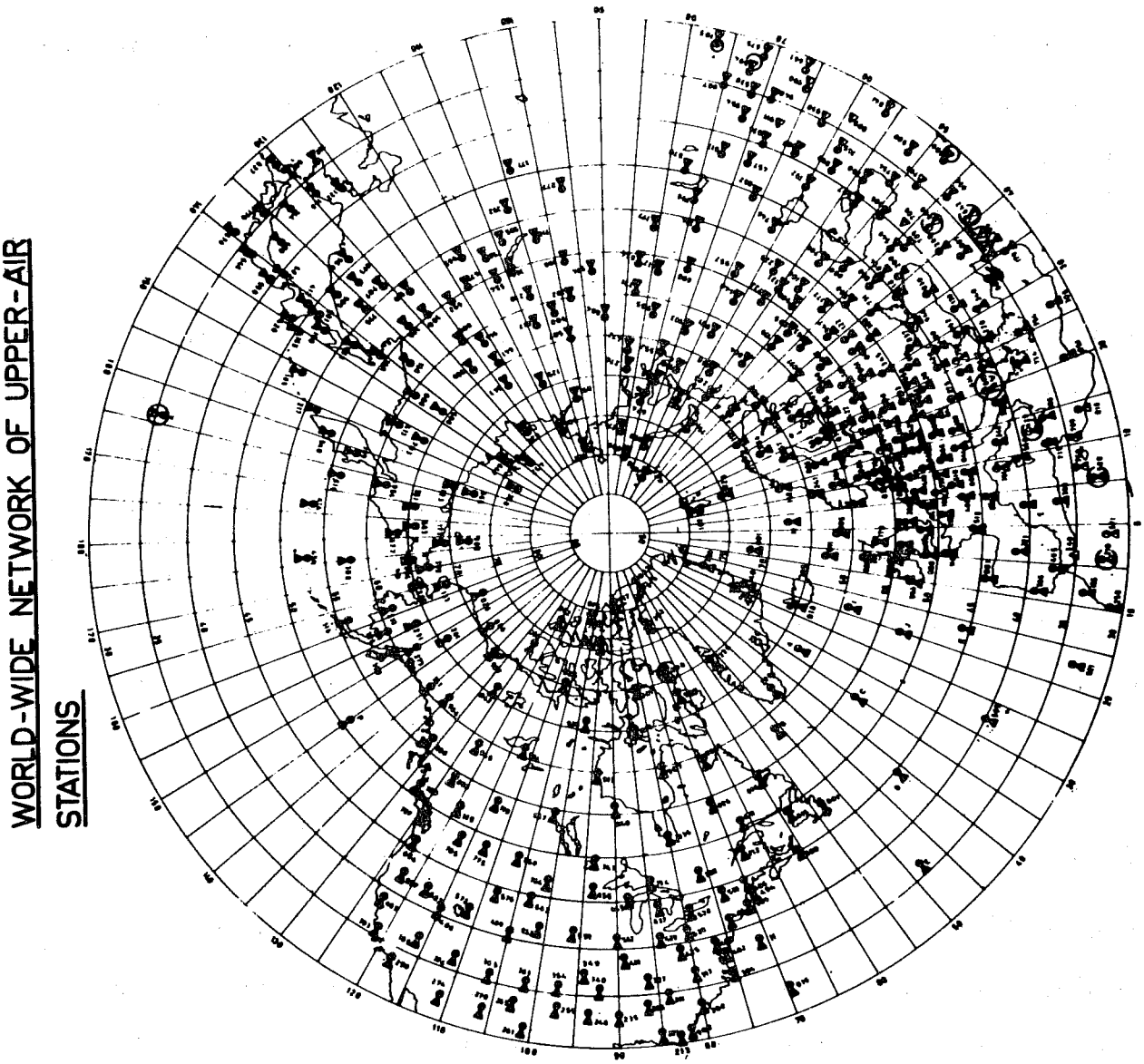

Fig. 1 (Ch.1)

W.W.W. upper air meteorological observation station in Northern Hemisphere (extratropics only).

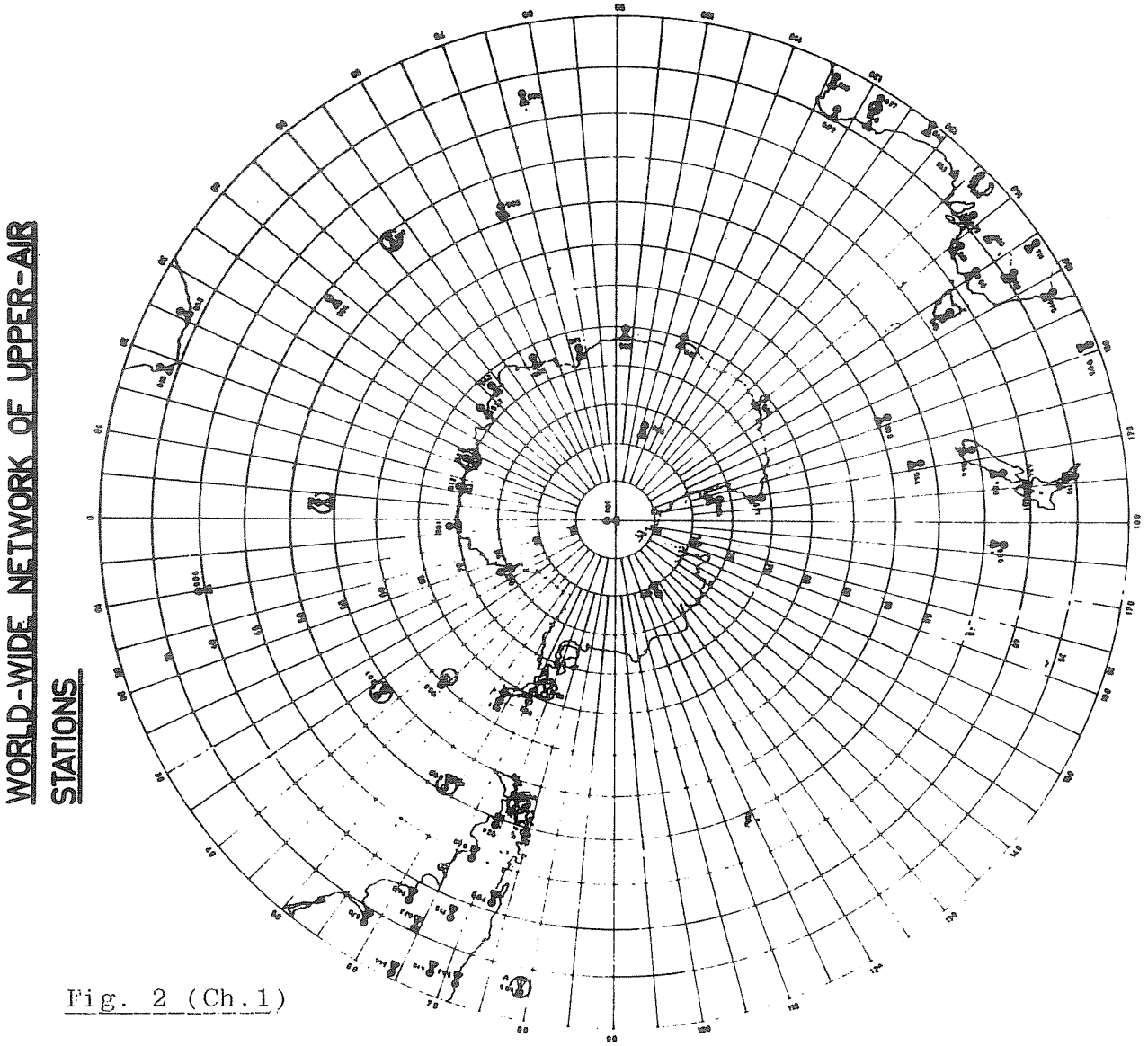

Fig. 2 (Ch.1)

W.W.W. upper air network in the Southern Hemisphere.

from adequate over oceanic areas, despite great international efforts to maintain a fair number of meteorological frigates in the Northern Atlantic and Northern Pacific. The situation is far from being as satisfactory in the Southern Hemisphere (fig. 2) as could be inferred from geography.

The most striking characteristics of the World Weather Watch ground based observation system is that it does not provide an homogeneous global coverage of the planetary atmosphere; nor is there any serious chance that further upgrading will produce such global coverage: that problem is just too vast to be tackled within reasonably economical bounds by a large extension of ground based observations. Thus, another characteristic of the present day Global Observing System is that of being in a stage of transition between purely ground based synoptic observations acquired at 00 and 12 GMT, and a mixed system incorporating a vast amount of non-standard, non-synoptic data inferred from remote observations obtained by meteorological satellites.

Communications and timeliness

Western european meteorologists are generally quite conversant in modern communication techniques and they have turned their data acquisition and collection system through national and regional centres or "communication hubs" to such a high degree of performance and reliability that they think nothing of imposing a

two to four hour deadline for observations used in regional forecasts. They have however, together with experts from industrial countries, applied the same concept to the collection of global data sets, in spite of vastly different conditions of communication facilities around the world. The resulting WWW Global Telecommunication System (fig.3) is indeed a powerful and constantly improving network, but it would be a mistake to expect that it will ever operate as specified in the book. Recent statistics compiled by the Washington World Meteorological Centre at the request of the Joint Organizing Committee for GARP indicated that at the best reporting hour (1200 GMT) less than 33% of the planned 500mb observations and 25% of 200mb observations from 30 tropical stations in Africa were reported in time to be included in the global analysis.

An even more difficult problem is met for collecting observations at sea from several thousand selected merchant vessels or "ships of opportunity". These meteorological observations, generally excellently made, do more often than not get lost in the process of transmission (on a voluntary basis) on ship-to-shore radio and never find their way in the meteorological channels. Statistics of marine traffic indicate that all 5^{o} by 5^{o} square of the Northern Oceans is occupied by at least one merchant vessel at any one time, so that a complete and homogeneously dense determination of the atmospheric pressure field could be assembled every day if barometric measurements from all these ships could be communicated in time. Such is the scope of the information we are presently

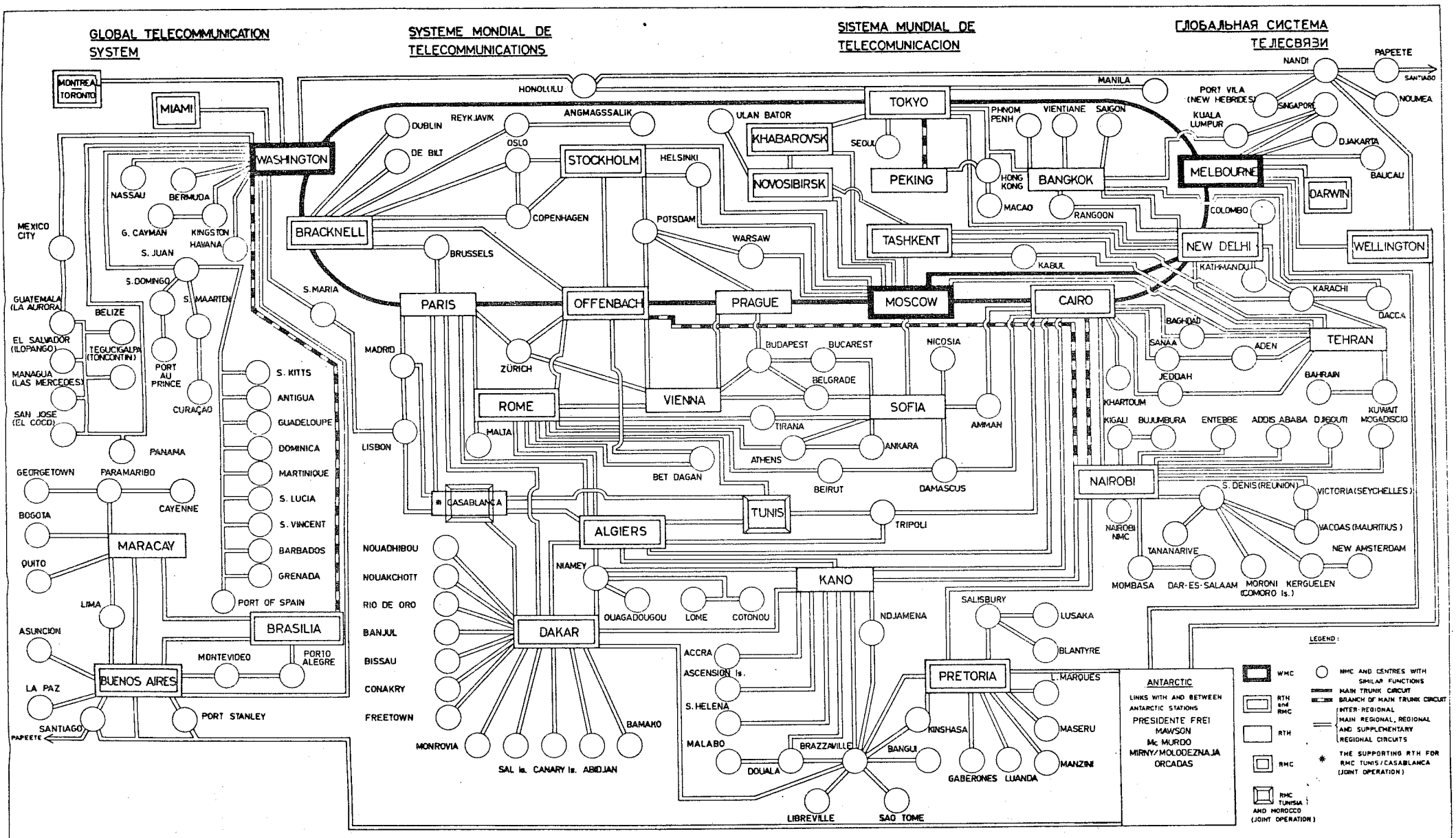

The designations employed and the presentation of the material on this map do not imply the expression of any opinion whatsoever on the part of the Secretariat of the World Meteorological Organization concerning the legal status of any country or territory or of its authorities, or concerning the delimitation of its frontiers.

Les désignations utilisées dans cette carte et la présentation des données qui y figurent n'impliquent de la part du Secrétariat de l'Organisation météorologique mondiale aucune prise de position quant au statut juridique de tel ou tel pays ou territoire, ou de ses autorités, ni quant au tracé de ses frontières.

Las denominaciones empleadas en este mapa y la forma en que aparecen presentados los datos que contiene no implican, de parte de la Secretaría de la Organización Meteorológica Mundial, juicio alguno sobre la condición jurídica de ninguno de los países o territorios citados o de sus autoridades, ni respecto de la delimitación de sus fronteras.

Употребленные на этой карте обозначения и оформление материала не должны рассматриваться как выражение какого бы то ни было мнения со стороны Секретариата Всемирной Метеорологической Организации относительно правового статуса той или иной страны или территории или ее властей, или относительно делимитации ее границ.

Fig. 3 (Ch. 1)

losing through the lack of appropriate communication channels. Thus a further conclusion we may draw is that we are indeed in need of a fast worldwide data collection system, based obviously on suitable (dedicated) space relays. It is gratifying to note that at least two such systems will be implemented in the near future (data collection system on four geostationary satellites around the Equator, and ARGOS data collection and location system on the TIROS-N operational satellite series).

Accuracy and representativity

Following the basic discovery of Torricelli, natural scientists and later meteorologists have constantly perfected the measurements of atmospheric pressure. Thus surface pressure is currently reported to the next 0.1 mb, a fantastic precision (10^{-4}) for a routine environmental measurement. This apparent precision should however be qualified in some circumstances. Dynamic effects associated with the disturbance of the air flow caused by obstacles are usually negligible on well-built land stations, but not however on an island or a ship at sea. Different practises for compensating dynamic pressure effects led recently to a 0.3 mb discrepancy between USSR and US research vessels which participated in GATE. A further difficulty occurs in the equatorial zone subject to a significant semi-diurnal pressure oscillation associated with the atmospheric tide. This pressure wave ($\pm$2 mb in the Indian Ocean) is an effect of solar heating and therefore locked on local solar time. Yet, pressure reports are synchronized on universal time, thus yielding an instantaneous picture of the pressure wave

which may overshadow the weak synoptic pressure gradient. This difficulty could obviously be removed by a proper application of sampling theory but this is not presently done.

The perfection of the radiosonde in the early 30's provided the meteorologists with a most powerful tool for analysing the thermal stratification of the atmosphere. Capitalizing on the progress made in fabrication of very sensitive thermistors (temperature dependent resistors), remarkably rugged yet precise radiosonde equipment have been produced and used in routine operation under the most adverse weather conditions: 0.5C precisions are claimed and even demonstrated in the troposphere and lower stratosphere. But it would be naive to expect such performance in the upper leg of a radiosonde ascent. As soon as the ambient pressure decreases below 30-50 mb and the molecular mean free path increases to a noticeable fraction of the diameter of the sensing element, the cooling capacity of the air flow decreases sharply and the relative importance of solar heating increases accordingly. Intercomparisons of radiosondes from different manufacturers are known to indicate discrepancies as large as 3C in the upper stratosphere (and worse for rocket soundings).

Finally, the observation of upper air winds is by far the most difficult and possibly the least significant measurement which could be made from the ground. One cannot in the first place put too much reliance on the lower level wind data because the wind structure in the planetary boundary layer is quite often subject to

quite large diurnal variations which are very significant with regard to local weather but not significant on the planetary scale. One cannot place too much confidence in the upper altitude winds either because of systematic failures to report the fastest winds due to a loss of tracking at very low elevation angle. Compare for example 200 mb wind velocity statistics compiled from EOLE constant level balloon velocity data in the Southern Hemisphere with conventional radiowind or radarwind data. Figure 4 shows a typical radar wind profile compared with the corresponding navigational sonde (Omega sonde) data. Note the scolloped appearance of both profiles which is characteristic of a distinct layering of the atmospheric flow but also, of significant measurement errors, of the order of 1-2 m sec^{-1}. Highly accurate radar tracking experiments were conducted by the US Air Force in an effort to distinguish between genuine atmospheric wind structures and aerodynamically induced motions of the balloons. These trajectories exhibited decidedly kinky appearance (Fig.5) indicating the existence of semi-periodic balloon motions during the ascent. Such aerodynamically induced motions were finally eliminated by using special high rugosity spherical balloons (or "Jimsphere") thereby approaching the ultimate precision limit of wind sensing. The result was that atmospheric turbulence places a $\pm$2 to 3 m sec^{-1} uncertainty on any instantaneous wind measurement in the troposphere, and that persistent vertical shears in the stratosphere introduces local discrepancies as large as $\pm$5m sec^{-1} within a 500 m layer.

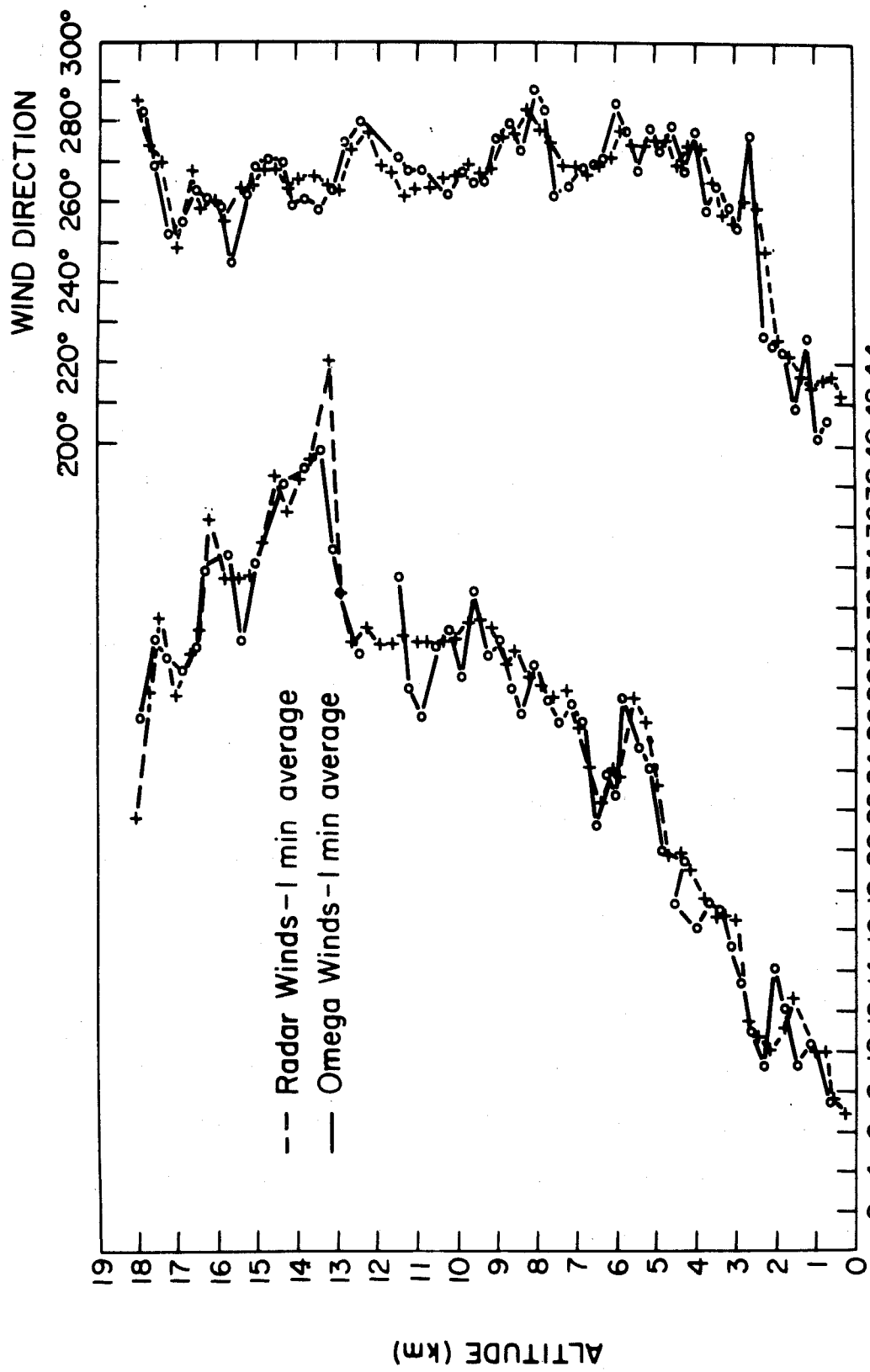

Fig.4 (Ch.1)

Comparison of radar tracking and navigation by Omega V.L.F. signals for one typical radiosonde ascent

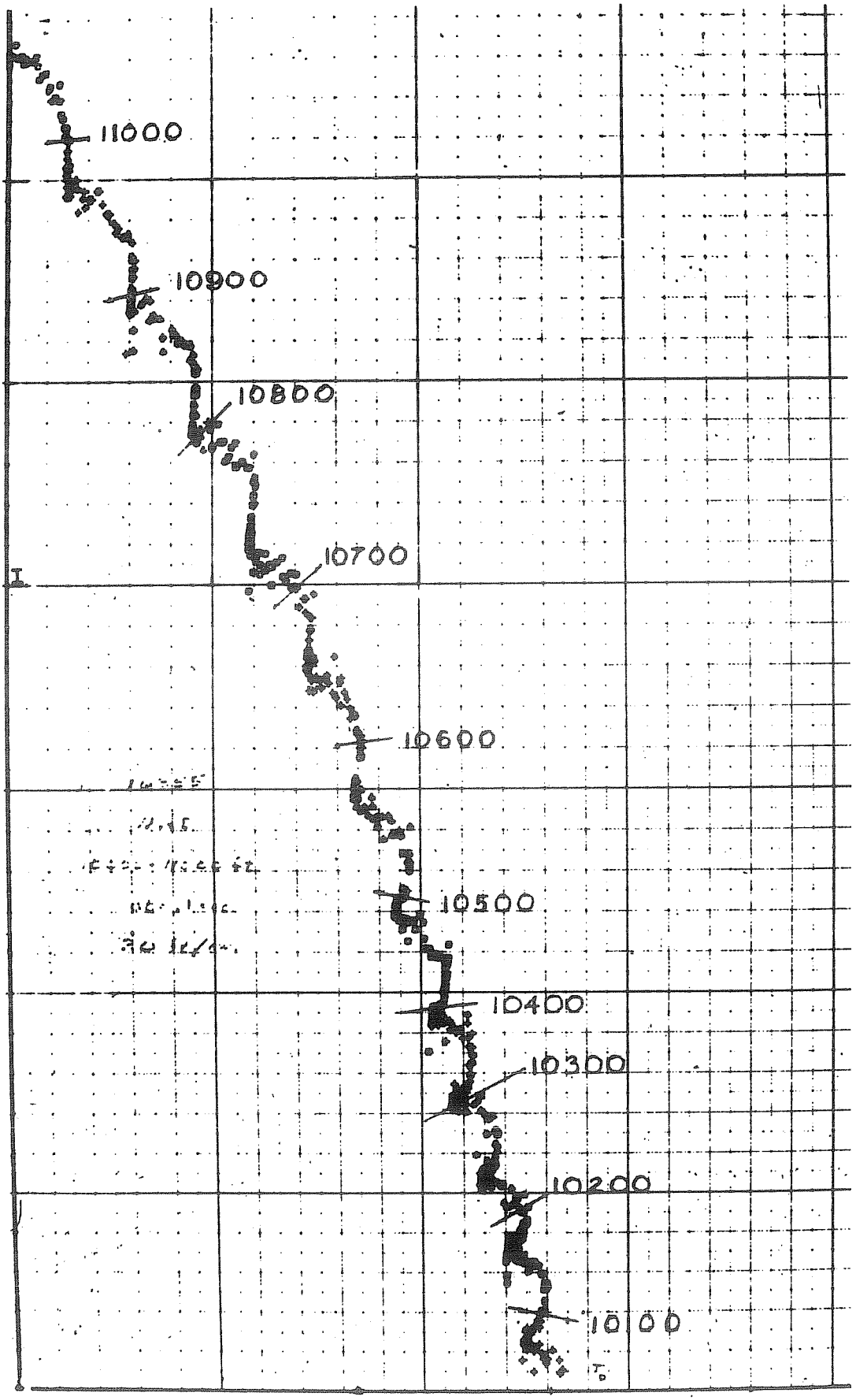

Fig. 5 (Ch.1)

High accuracy radar determination of the trajector of an ascending balloon

Level of Data Processing

Because the WWW global observing network is evolving toward a complex system mixing a variety of direct and indirect (remote) observations of atmospheric processes, it has become necessary to refine our glossary of terms for defining the various stages of data processing. The following vocabulary has been developed mostly in the perspective of remote sensing techniques from space but it applies in principle to any measurement.

Now we refer as Level I data to calibrated readings of the primary physical quantity measured by the instrument (e.g. radiation fluxes for a space borne radiometer) expressed in universal physical units (e.g. watts/m^2) after taking into account all instrumental characteristics such as field of views, spectral bandwidth, detector calibration and telemetry encoding. Such data are valid measurements by themselves but do not necessarily correspond to one particular meteorological parameter.

It is possible, however, on the basis of mathematical analysis and/or statistical (empirical) consideration, to "infer" from level I data,estimates of meteorologically significant parameters such as the temperature profile or moisture content of the underlyi atmosphere, for example. This processing will therefore yield an estimate of meteorological quantities referred to the particular place (x, y, z) and time t of the original observation. Such estimates are known as Level II data.

Finally, it is appropriate to assemble all available meteorological parameter values collected during one period of time (12 or 24 hours) into one single consistent picture of the global atmosphere at one single synoptic time, as needed for initializing a forecast of future evolution. This process based on space-time interpolation or more refined techniques for optimizing the static and dynamic consistency of the data, is called analysis. The products, are Level III data, i.e. mutually consistent, complete sets of the basic dynamical variables referred to one single map time and standard grid coordinates or any similar representation of the meteorological fields.

It is the purpose of this series of lectures to explore these two steps of meteorological data processing: how to infer level II meteorological data from raw (level I) physical measurements, how to analyse sets of individual meteorological observations distributed randomly in space and time for producing consistent level III meteorological fields.

References

. The First GARP Global Experiment: Objectives and Plans, GARP Publication Series No.11 (1974).

. Report on Special Observing Systems for the First GARP Global Experiment. GARP Special Report No.10, 1973.

2. Cloud and Surface Observations from Space

The year 1975 marks the fifteenth anniversary of the first meteorological satellite TIROS 1 which produced the first television pictures of the earth surface and weather systems. Within a few days of the launch of TIROS-1 these raw data were being used operationally by meteorologists to improve qualitatively the weather maps and nephanalyses. In the ensuing years, many types of television and finally high resolution scanning radiometers were developed, together with progressively more sophisticated techniques for exploiting these pictures from space.

Experienced analysts have from the very beginning been able to recognize the significant cloud patterns and associate them with the development of weather systems such as fronts, tropical disturbances and obviously hurricanes. It was nevertheless a shock to this lecturer to find out that the subjective analysis of these qualitative cloud images from space has been perfected to such a high degree of accuracy and reliability that "bogus" surface pressure and 300 mb geopotential data over oceanic areas are produced routinely by experienced human analysts and fed to the computer with remarkably good results: such good results in fact that the replacement of these "bogus data" by the first objective determination of temperature profile obtained by remote sensing (VTPR data) showed very little if any improvement.

Qualitative image data from orbiting (sun-synchronous) and geostationary satellites have become so directly useful for local weather surveillance and short term forecast that the acquisition

and analysis of satellite pictures is now almost as typical a fact of the meteorologist trade as looking over the barometer. Picture data transmitted in real time according to the Automatic Picture Transmission (APT) scheme are received by hundreds of stations operating throughout the world. But this aspect of satellite data utilization does not relate with the major topic of this seminar, i.e. extended forecast of the planetary atmospheric flow.

Sea Surface Temperature

The first attempt to derive quantitative measurement from space imagery was the determination of sea surface temperature from infrared images obtained at night in the 3.4 to 4.2μm spectral window by the High Resolution Infrared Radiometer (HRIR) mounted on Nimbus-2. Accuracy was quite marginal for most oceanographic purposes but yet adequate for delineating the boundary of the Gulf stream off Cape Hatteras ($\pm$3C). Major technological efforts and data processing refinements have been necessary to compensate for air and water vapour absorption, instrumental noise, cloud contamination of the field of view and bring the RMS difference between space based and ship measurements just under 1C (Shenk and Salomonson, 1972 ; Prabhakara, 1974).

The development of much more sensitive infrared detectors and very high resolution thermal infrared imagery (VHRR), as well as better remote estimates of the water vapour content of the atmosphere bear the promise of still reducing the two major sources of errors for the remote measurement of sea surface temperature, i.e. contamination by clouds and absorption by water molecules.

Sea Surface Stress

The feasibility of measuring the sea surface roughness and surface stress was demonstrated by Levanon (1971) by using sun glitter measurements from a geostationary satellite. But more recently, 15 millimeter radiance data measured by the Nimbus 5 Electrically Scanning Microwave Radiometer (ESMR) have been used to infer realistic surface wind speed gradients in the Mediterranean under a variety of weather conditions, while measurements of scattered microwave radiations from Skylab over Hurricane Ava in 1973, yielded a confirmation of the approximate square law relation between the scattering coefficient for horizontal polarization and the wind speed. There is no doubt that further development of both active and passive microwave probing of the oceans will eventually yield reliable estimates of the wind stress and thereby open a new era for real time ocean dynamic studies (as needed to further the second GARP objective).

Heat budget of the Earth-Atmosphere System

Many studies have now been performed to analyse the measurements of emitted long-wave and reflected solar radiation acquired by medium resolution scanning radiometers such as MRIR on Nimbus 3 and the Earth Radiation Experiment on Nimbus 6 and also by a variety of simpler spherical or flat plate radiometers flown on both experimental and operational satellites since 1962. Von der Haar and Suomi (1971) reported the first satellite measurements of the planetary albedo and radiation budget from 39 months of data in the 1962-66 period. They found that the earth-atmosphere system

is generally warmer (255 K vs. 250 K) and darker (29% albedo vs. 35%) than previously believed. Von der Haar, Raschke and colleagues also showed that most of the radiative energy input in excess of the older results was received by the tropical regions, thus requiring a larger poleward energy transport than previously believed. This led Von der Haar and Oort (1973) to combine the radiation budget data with atmospheric energy transport data to derive a revised value of the transport of sensible heat by ocean currents between equator and pole, now estimated to be 40% of the total poleward transport.

These studies are certainly beyond the scope of the present medium range weather forecast objective. But they provide the most reliable information on the long term energy balance of the planet and possibly some insight is the cause of climatic fluctuations. Note for example an intriguing result of Kukla and Kukla showing that the recent anomalous global weather pattern most dramatically highlighted by drought in the Sahel region, coincided with a significant extension of the snow and pack-ice cover of the Northern Hemisphere producing in turn a significant change in the hemispheric heat balance.

Finally, it is worthwhile mentioning that even though radiometric instruments in orbit are not quite precise enough nor widely enough distributed over all possible illumination conditions to provide reliable instantaneous values of the synoptic scale radiation budget, there is presently a forceful drive to achieve

a better calibration and a better sampling of the net radiative fluxes to the point of allowing a useful comparison with the calculated energy budget of operational general circulation models.

Cloud parameter measurements

A large and multi-pronged attack is being conducted around the world on the quite difficult problem of automatic nephanalysis: how to recognize cloud types, density and altitude (temperature) on the basis of relatively coarse imaging and wide-band multispectral data. Several techniques based on visible (reflected light) brightness and/or IR window measurement, and more recently water vapour absorption band imagery (Allison and Steranka, 1972) are being studied by many investigators with increasingly promising but not fully satisfactory results. Nevertheless, the U.S. Air Force now produces routinely a global daily nephanalysis based essentially upon satellite imagery and the known thermal stratification.

References

1. Allison and Steranka, Bull. Am. Meteo. Soc. 6, pp. 526-535, (1972)

2. Kukla and Kukla, Science, 183, pp. 709-714 (1974).

3. Levanon, J. Phys. Ocean, 1, pp. 214-220 (1971)

4. Prabhakara, Daler and Kunde, Document X-911-711-60, Goddard Space Flight Center, (1974).

5. Sabatini EPRF Tech. Report 5-74, The Earth Satellite Corporation, Washington, (1974).

6. Shenk and Salomonson, J. Phys. Ocean. 2, pp. 157-167 (1972).

7. Von der Haar and Oort, J. Phys. Ocean, 3, pp. 169-172 (1973).

8. Von der Haar and Suomi, J. Atmos. Sci. 28, pp. 305-313 (1971)

3. Air Temperature and Moisture Observations from Space :

PART I: The inversion problem

The possibility of inferring the vertical temperature structure of the atmosphere from satellite measurements of the spectral radiance in the 15 μm absorption band of carbon dioxide was first suggested by Kaplan (1959). On the basis of Kaplan's suggestion, two instruments were developed to be flown on Nimbus 3 in 1959. These were the Satellite Infra Red Spectrometer (SIRS) and Infrared Interferometer Spectrometer (IRIS). These pioneering experiments did confirm the feasibility of retrieving useful temperature information from purely spectrophotometric measurements in outer space but also indicated many problem areas pertaining to absolute radiometer calibration in space, uncertainty about the true transmittance of the atmosphere in the CO_2, H_2O and O_3 bands as well as the impact of scattered cloudiness within the field of new of the instruments. Finally much fundamental work was needed to fully understand and perfect the mathematically questionable procedure of profile inversion. Most of these tasks have now been completed and we may consider that the remote determination of the atmosphere temperature field is a proven technique which is implemented routinely and compares not too unfavourably with conventional in-situ measurements.

Theoretical Background

The simplest case to consider is the retrieval of the temperature profile of a cloudless atmosphere resting on a black-body surface. We generally assume that the CO_2 is mixed well enough so that atmospheric composition can be taken unvariant with time and place. Actually this is only a first order approximation since the amounts of other minor constituents such as water vapour and ozone are highly variable and modify the atmospheric transmittance even in the CO_2 emission band. In effect, the transmittance of the mixture must be estimated using climatology or a n independent measure of the water vapour content. We shall disregard this complication for the moment.

Let us consider then that the mass absorption coefficient $k(\nu)$ in a narrow spectral interval centered at ν, is exactly known for the standard mixture of air and CO_2. Let us assume further a cloud free, plane-parallel atmosphere in which temperature T(p) is uniform in each horizontal plane. The outgoing radiation flux $I(\nu,p)$ crossing the pressure level p obeys then the differential relation :

$$dI(\nu,p) = I(\nu,p) - B(\nu,T(p))\ k(\nu)\ dp/g \qquad (1)$$

where $-I(\nu\ p)\ k(\nu)\ dp/g$ is the differential fraction of the outgoing flux absorbed in the air mass dp/g, while $k(\nu)$ $B(\nu,T)\ dp/g$ is the radiation emitted by the same air column. $B(\nu,T)$ is the Planck radiance function for a black body, appropriate to wave number ν and temperature T. Equation (1)

can be simplified by introducing the alternate vertical coordinate x such that :

$$x = \int_o^p k(\nu)\, dp'/g$$

Disregarding for the moment the wave number dependence, equation (1) is written :

$$dI = \left[I(x) - B(x) \right] dx$$

which can be integrated from the surface x_s to the top of the atmosphere (p=x=o) yielding :

$$I = B(x_s)\, e^{-x_s} + \int_o^{x_s} B(x) e^{-x}\, dx \qquad (2)$$

Equation (2) is more conveniently written by introducing the fractional transmission $\tau(\nu,p)$ for the spectral interval centered at wave number ν, between the top of the atmosphere (p=o) and pressure level p. Thus

$$\tau(\nu,p) = e^{-x} \qquad (3)$$

Introducing (3) in relation (2) one gets the basic transfer equation :

$$I(\nu) = B(\nu,T_s)\, \tau(\nu\, p_s) - \int_o^{p_s} B(\nu,T(p)) \frac{d\tau}{dp}\, dp \qquad (4)$$

where the vertical coordinate p can also be replaced by any

single valued function x (p); $d\tau/dp$ is known as the weighting function for outgoing radiation at wave number ν It is obviously a strongly dependent function of k (ν) as shown in Fig. 1 and 2.

The integral equation (4) implicitly involves the temperature profile T(p) to determine the outgoing long wave radiation spectrum. Obviously, if the weighting function $d\tau/dp$ peaks at some high level of the atmosphere where the temperature is low, the apparent planetary temperature is rather low and the observed radiance is small. Conversely, if the weighting function peaks at a low altitude where temperature is fairly high, the apparent planetary temperature is also high and the observed radiance is large. The possibility of actually solving the inverse problem i.e. determining the temperature profile T(p) from known values of radiances I (ν) at various wave numbers, (Fig.3) relies on the fact that the weighting functions peak within a fairly narrow atmospheric layer (Fig.2), so that a variety of simplifications can be applied, all being equivalent to solving a linearized version of integral equation (4). In the first place, we notice that the Planck function is not going to change much as the wave number is shifted through the useful range 668 to 750 cm^{-1} from the center to the wing of the CO_2 absorption band. But the Planck function will be rather sensitive to meteorological temperature variations from top to bottom of the atmosphere, because it is large in relative value. On the other hand, the difference at any one level x between temperature, T(x) on one particular day and a first guess $\bar{T}(x)$ based on climatology, a previous

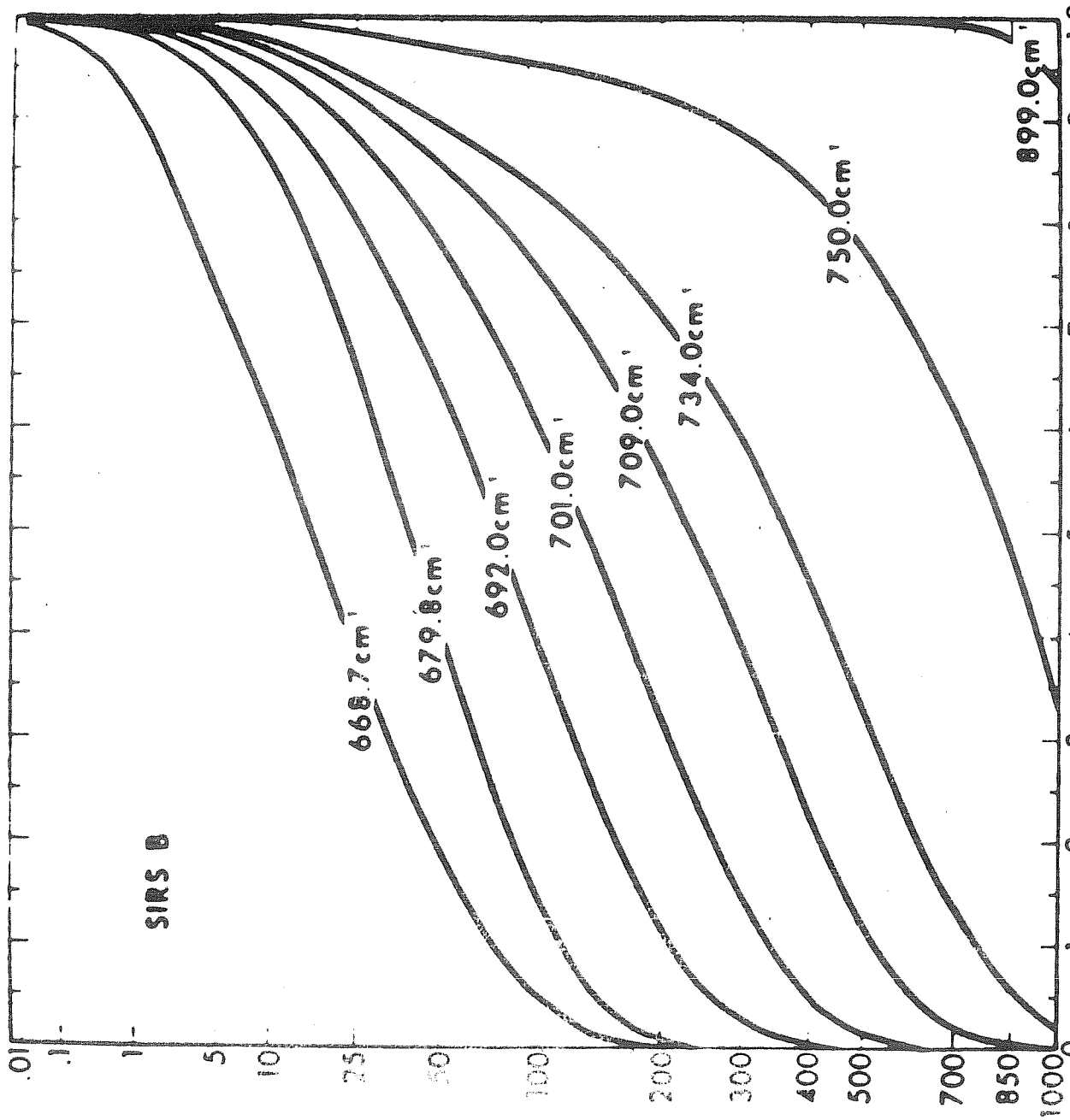

Fig.1 (Ch.3) Variation of atmospheric transmittance with depth and the wave number of the spectral channel.

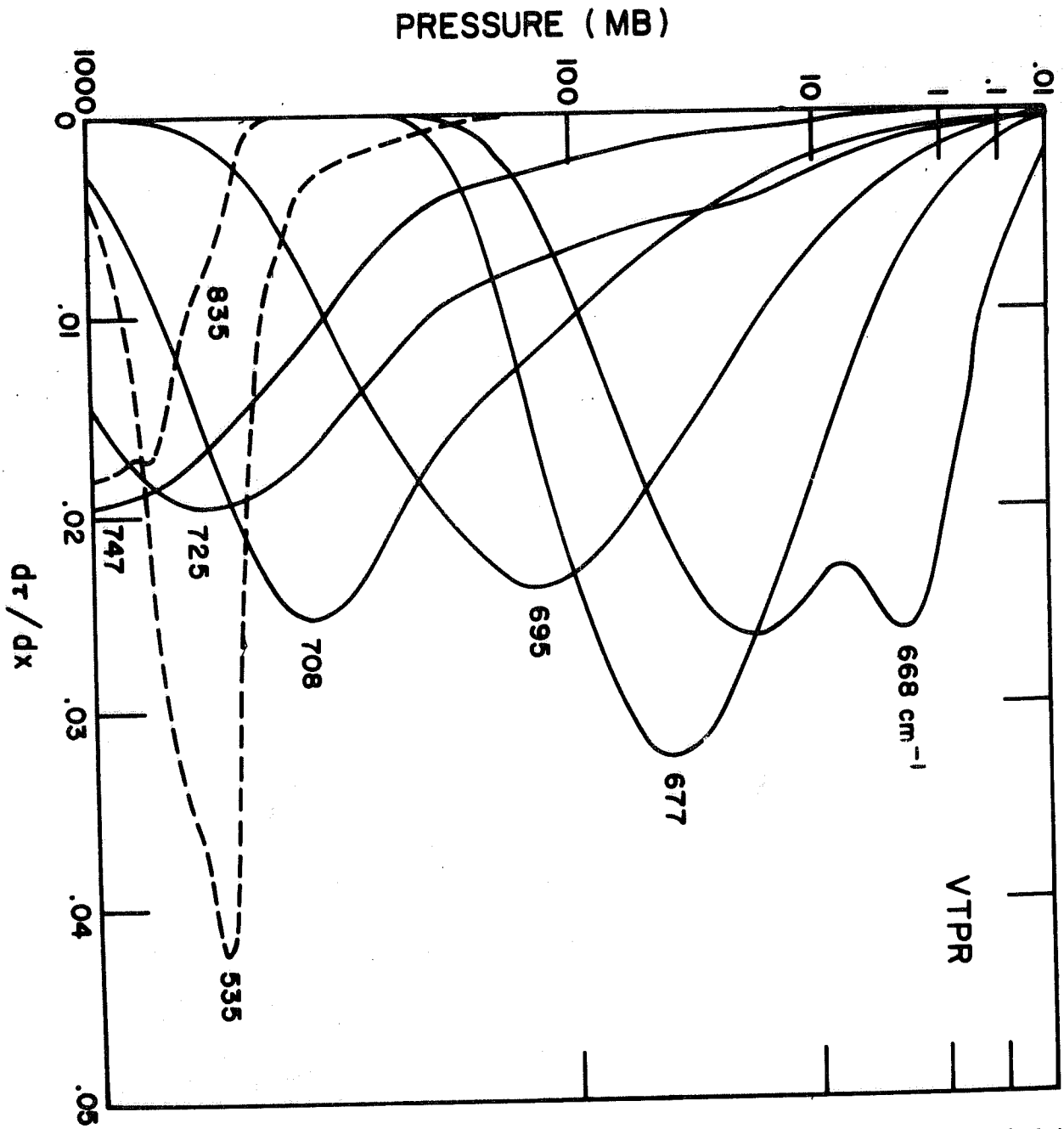

Fig.2(Ch.3)

Weighting functions dτ/dp for 6 channels within the CO_2 band, and the water vapour band channel of the VTPR instrument on NOAA operational spacecrafts.

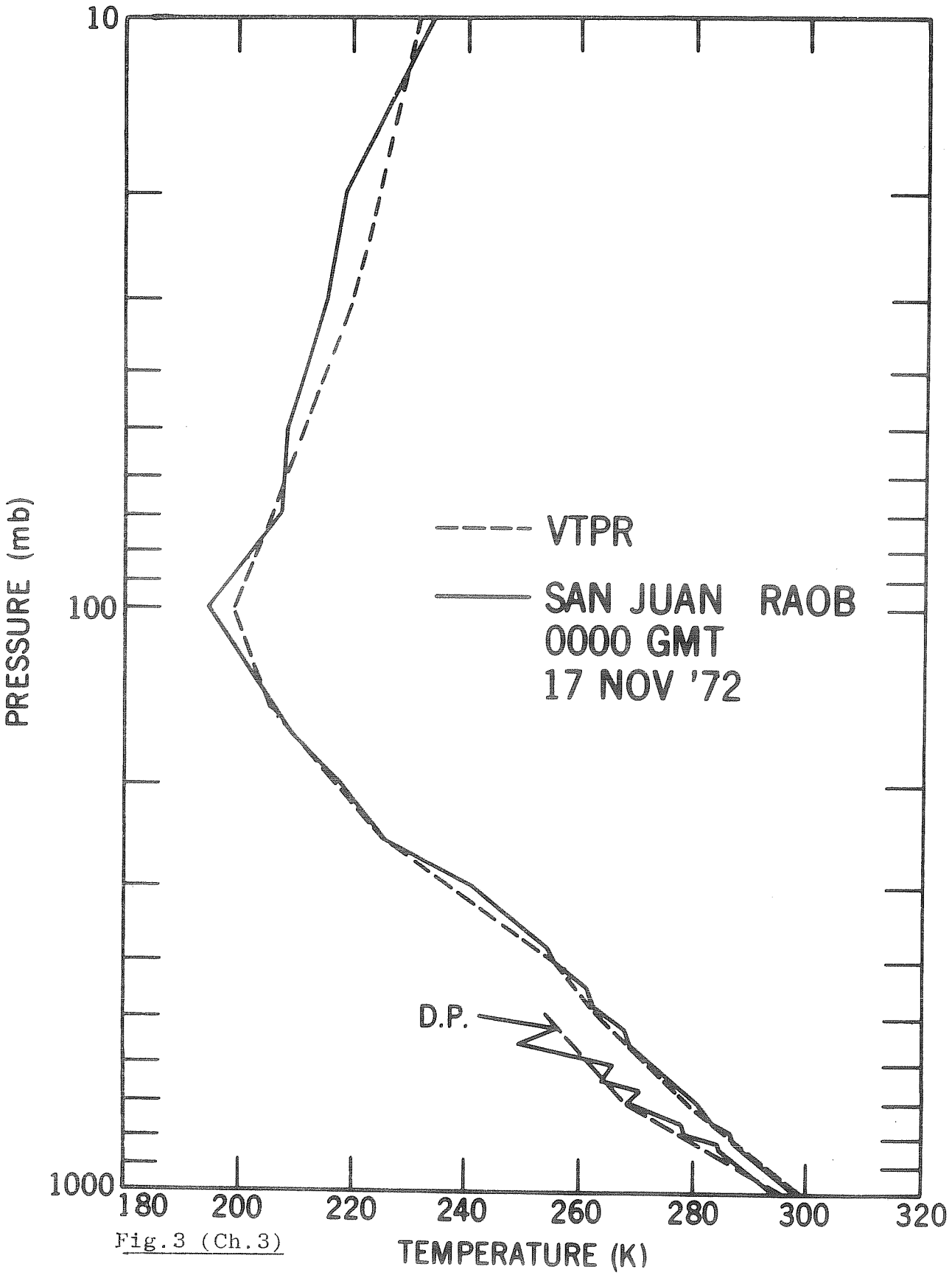

Fig.3 (Ch.3)

Typical temperature and moisture profile obtained by inversion of VTPR spectrometric data, compared with coincident radiosonde measurements.

forecast or most generally anything convenient, is not likely to be very large and can be considered as a small variable in relative value (1 - 2 % of absolute temperature).
Thus it is helpful to measure the instantaneous temperature in a term of difference of the Planck function at a standard wave number ν_o = 700 cm^{-1} say:
We introduce then the new variable :

$$b(x) = B\left[\nu_o,\ T\ (x)\right] - B\left[\nu_o,\ \bar{T}\ (x)\right] \qquad (5)$$

and the (approximately) known function :

$$\alpha(\nu) = \frac{B\ (\nu,T) - B\ (\nu,\bar{T}\ )}{B\ (\nu_o,T) - B\ (\nu_o,\bar{T})} \approx \frac{dB(\nu,\bar{T}\ )/dT}{dB(\nu_o,\bar{T})/dT} \qquad (6)$$

Using definitions (5) and (6) yields the approximation :

$$B(\nu,T) = B(\nu,\bar{T}\ ) + \alpha(\nu)\ b(x) \qquad (7)$$

where the wave number dependence and the temperature dependence (through b(x)) are separated. It is straightforward to show that this approximation yields a linear version of (4) .
Indeed :

$$I(\nu) = B\ (\nu,T_S)\ \tau(\nu,x_S) - \int_o^{x_S} \left[B(\nu,\bar{T}\ ) + \alpha(\nu)\ b(x)\right] \frac{d\tau}{dx}\ dx \qquad (8)$$

And simultaneously for the first guess profile (the surface black body temperature T_s must be determined independently) :

$$\bar{I}(\nu) = B(\nu, T_s)\, \tau(\nu, x_s) - \int_0^{x_s} B(\nu, \bar{T})\, \frac{d\tau}{dx}\, dx \qquad (8')$$

Subtracting (8') from (8) yields an expression for the residue $r(\nu)$:

$$r(\nu) = I(\nu) - \bar{I}(\nu) = -\int_0^{x_s} \alpha(\nu)\, b(x)\, \frac{d\tau}{dx}\, dx$$

and finally lumping together the two known functions $-\alpha(\nu)$ and $d\tau/dx$ into one kernel $K(\nu)$ we get :

$$r(\nu) = \int_0^{x_s} K(\nu)\, b(x)\, dx + \Sigma(\nu) \qquad (9)$$

The purpose of the incremental quantity $\Sigma(\nu)$ is to give an explicit representation to the errors (or noise) in the measurements of the spectral radiance $I(\nu)$. (9) is a regular Fredholm linear integral equations for each spectral channel $\nu_1, \nu_2, \ldots \nu_M$ of the radiometer. Assuming that we want to solve the inverse problem for N discrete equal weight atmospheric layers (in x coordinate), the integral equation (9) is replaced by a set of M standard linear equations

$$r(\nu_i) = \sum_{j=1}^{N} K(\nu_i) b(xj) + \varepsilon(\nu_i)$$

or in matrix form :

$$r = Kb + \varepsilon \qquad (10)$$

where r and Σare M-dimensional vectors, b is a N dimensional vector and K is a M x N matrix.

Inverse Matrix Method

We may take advantage of the large quantity of atmospheric data already compiled and use temperature measurements which are coincident (in space and time) with satellite measurements so as to solve the inversion problem by the regression technique first proposed by Smith and colleagues (1970). Let R be an array of satellite radiance measurements for all M spectral channels and K different locations where simultaneous radiosonde measurements are available and E the corresponding noise.
Also let B be the KxN array of temperature measurements at N different levels in the same K locations. Thus :

$$R = KB + E \qquad (11)$$

The regression problem is then that of finding the M x N matrix C which best fits the relation:

$$B = CR$$

which would yield the actual temperature profiles, given the corresponding radiances. This matrix must be such as to minimize the distance ;

$$\| B - CR \| = tr \, (B - CR) \, (B - CR)^{T} \qquad (12)$$

Differentiating (12) with respect to the element of matrix C and setting the result equal to zero yield the solution :

$$C = BR^{T} \, (RR^{T})^{-1} \qquad (13)$$

as found in textbooks (Graybill, 1969) so that any particular solution can now be obtained from the equation:

$$b = Cr \qquad (14)$$

Iterative non-linear method

The most familiar of the non-linear methods is that by Chahine (1970) which really consists in applying the mean value theorem to the transfer equation (4). Consider first that B (ν,T) is a slowly varying function in the vertical interval of interest (O,x_s) while $\frac{d\tau}{dx}$ is a rapidly varying function with a peak around $x = x_i$

Obviously :

$$-\int_{o}^{x_s} \frac{d\tau(\tau,x)}{dx} \, dx = -\int_{o}^{x_s} d\tau = 1 - \tau \, (\tau , x_s)$$

Then there must exist one value y within the interval (O, x_s) such that

$$-\int_{o}^{x_s} B\left[\nu,\ T(x)\right] d\tau = B\left[\nu, T(y)\right]\left[1 - \tau(\nu,\ x_s)\right] \qquad (15)$$

Because $d\tau(\nu_i, x) / dx$ has a sharp maximum, it is likely that y be very near the altitude x_i of this maximum.
We have then from (4) and (5) :

$$I(\nu) - B(\nu,T_s)\,\tau(\nu,x_s) = B(\nu,T(y))\left[1-\tau(\nu,x_s)\right] \qquad (16)$$

A similar relation holds for the first guess temperature profile $\bar{T}$, except that the y is not necessarily the same even if it is still close to the maximum of the weighting function. If the surface temperature T_s is known and the radiance value $I(\nu)$ measured, if the transmittance of the whole atmosphere $\tau(\nu, x_s)$ can be computed and $B(\nu,\bar{T}(x))$ is assumed as a first guess, relation (16) yields a first step approximation of the Planck function near the weighting function maximum.

$$\frac{B(\nu,T(y))}{B(\nu,\bar{T}(y))} \simeq \frac{I(\nu) - B(\nu,T_s)\tau(\nu,x_s)}{\bar{I}(\nu) - B(\nu,T_s)\tau(\nu,x_s)}$$

and so on, using this first step estimate to start a second iteration of the same algebra.

These different inversion techniques are not equivalent obviously, as shown by Fig. 4. A modification of the inverse matrix method, based on linearizing the original equation of radiative transfer is currently the most accurate. Note however that all methods fail to a considerable degree in regions of the atmosphere where sharp changes of slope occur e.g. in the planetary boundary layer and at the tropopause. The accuracy in the upper stratosphere is particularly poor because only the wings of the weighting functions extend at this high altitude, thus making the retrieved temperature profiles very sensitive upon the first guess profiles (which are based on scarce and not too precise rocketsonde data). Tropopause definition has always been a troublesome point in remote sensing: the variability of tropopause level from profile to profile and the amplitude of the temperature inversion combine to create difficulties which have not been overcome with the relatively poor vertical resolution provided by the weighting functions. A similar situation also occurs near the surface with some hope of better retrieval by using the 4,3 µm CO_2 band together with the 15µm band for improving the vertical resolution.

It turns out also that retrieved profiles are very sensitive to small errors of the weighting functions. This is no trivial matter as line-by-line integration of the CO_2 and other gaseous constituent absorption spectra does not yield accurate enough values of the effective atmospheric absorption coefficient $k(\nu)$ for each spectral channel.

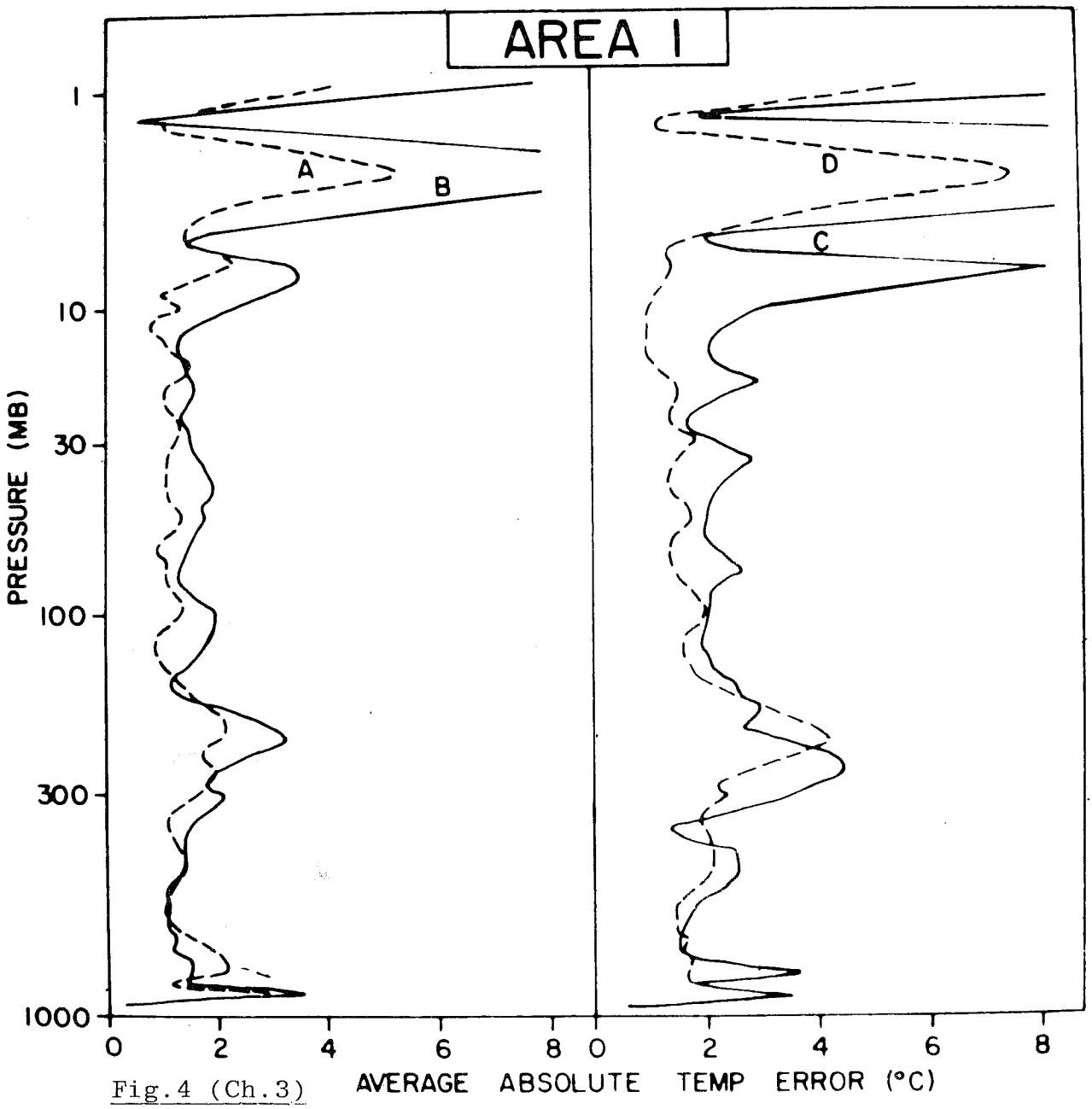

Fig.4 (Ch.3)

Inversion error statistics as a function of altitude for various inversion methods (A) stands for the inverse matrix method and (C) for the Chahine non-linear iterative method.

Nor is ground calibration satisfactory either because the shape of the spectral lines is in fact pressure dependent. Then in flight calibration or "tuning" is required to establish the most exact atmospheric transmittance and weighting function estimate, based on optimizing the correspondence between coincident in-situ temperature and moisture measurements, and radiance measurements. Fig. 5 is an example of this final in flight calibration of one channel of the ITPR spectrometer on Nimbus 5.

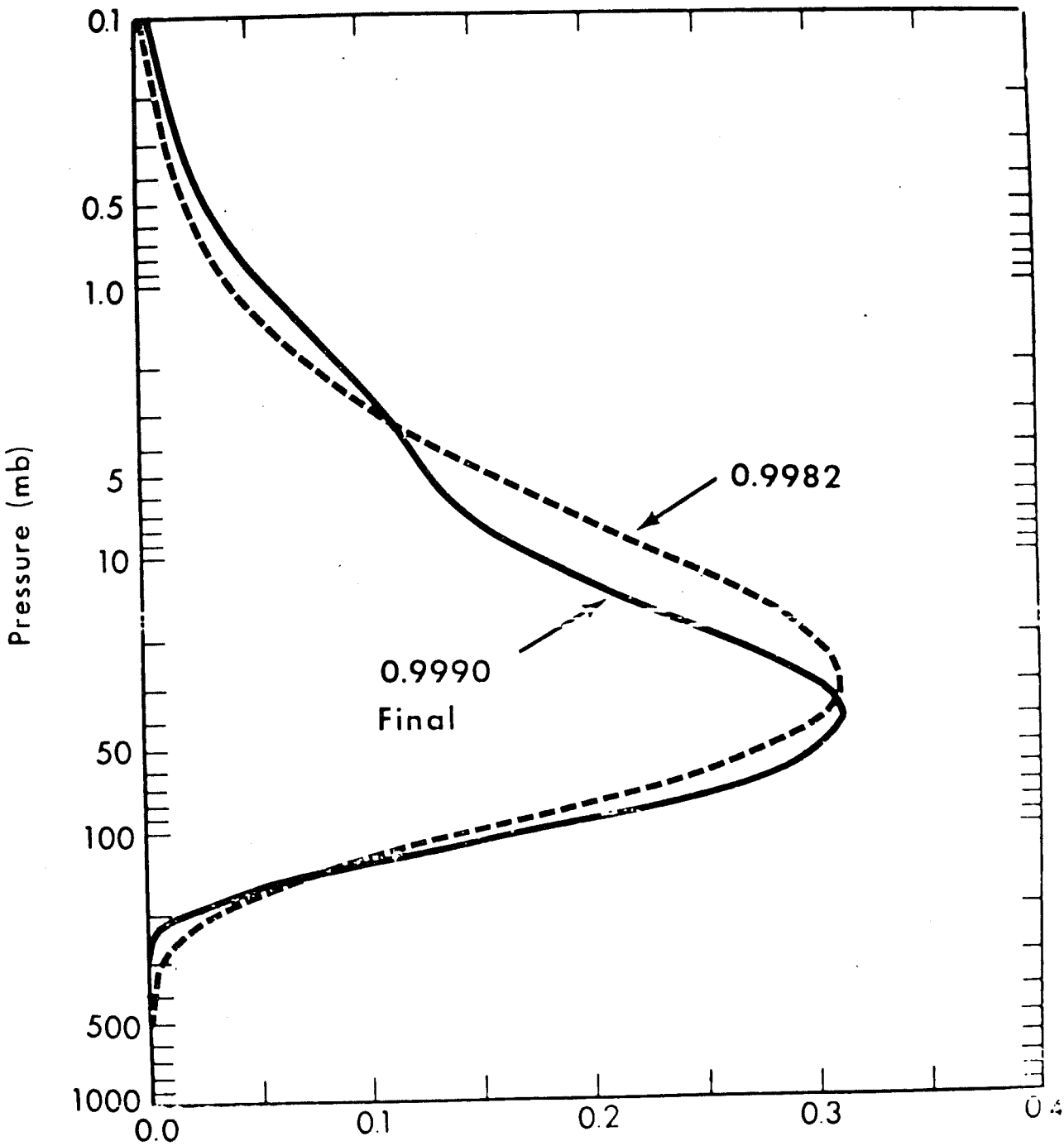

Fig.5 (Ch.3)

Initial estimate of the weighting function for the 668 cm^{-1} channel of ITPR , computed by line-by-line integration of spectrometric data, and final corrected estimate based on the optimization of 28 actual atmospheric profiles.

REFERENCES

1. Chahine, J. Atmos. Sci. 27, 960 (1970)

2. Graybill: Introduction to Matrices with Applications in Statistics. Wadsworth Pub.Co. 1969

3. Kaplan, J.Optical Soc.,America 49 pp 1004-1007 (1959)

4. Smith, Woolf and Jacob :
Monthly Weather Review, 98, 582 (1970)

For a more extensive bibliography see also "Temperature Sounding from Satellites " NOAA Technical Report NESS 59, Washington D.C. 1972

4. Air Temperature and Moisture Observation from Space

Part II: The instrumental problem

Beside this question of accurate absolute radiometric calibration of the radiometer instrument we touched upon in Part I, the most serious problem met with infrared temperature sounding spectrometer was that caused by the contamination of the field of view of the instrument by fractional cloudiness, e.g. broken opaque clouds and/or semi-transparent thin cloud layers. Note that such contamination is rather common occurance in the 200 km wide field of view of the VTPR instrument: in fact perfectly clear sky conditions are really the exception. The situation will be improved in the next generation, infrared spectrometers (already under test in Nimbus 5 and 6) with a much reduced instantaneous field ov view (30 km). Thus, one major initial step of radiance data processing is compensating for this cloud contamination effect and determining the radiance of the infrared radiation which would emerge from a column of clear air with the same temperature structure. Because clouds are highly variable in amount and characteristics, radiance measurements from neighbouring areas maybe widely scattered even though they all correspond to (essentially) the same temperature profile. However, since fractional cloudiness (x%) is the same for all spectral channels in the fairly narrow CO_2 emission band, the observed radiances obey the same linear relationship with x (see Fig.1).

$$I_{obs} = xI_{cloud} + (1-x)I_{clear}$$

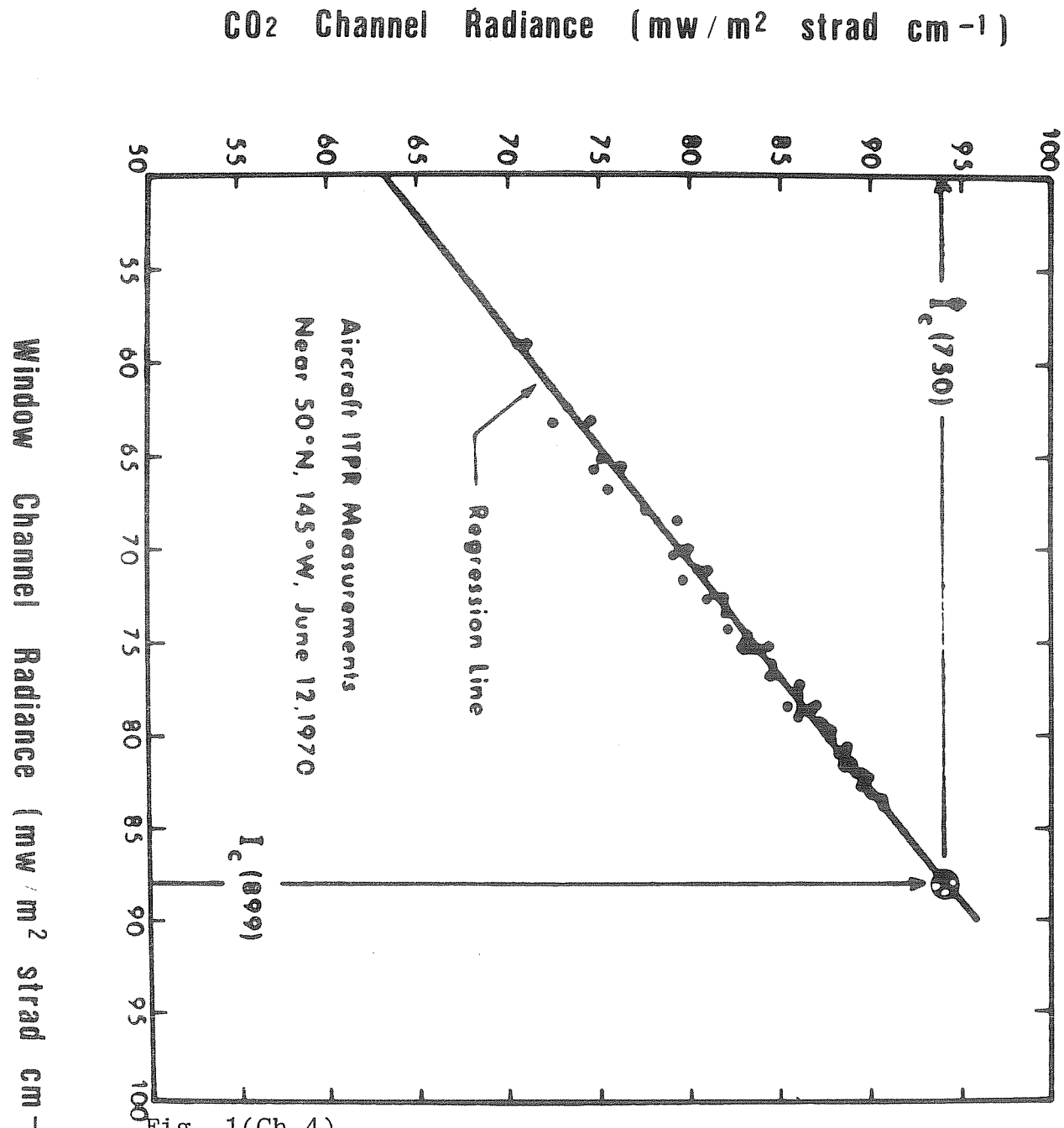

Fig. 1(Ch.4)

Linear relation of IR radiances measured simultaneously in two spectral channels, as a function of fractional cloudiness.

It remains to find the limiting value I_{clear} or clear column radiance which would be observed if fractional cloudiness were $x = 0$. This can be done if supplementary information is known such as a prior knowledge of the surface temperature T_s (e.g. climatological values at sea) or redundant spectral measurements are made such as simultaneous observations in the two atmospheric windows at 3.7μm and 11μm (Fig.2). Estimated clear column radiances will then be used as input to the inversion scheme as outlined in Part I, to retrieve essentially unaffected temperature profiles (Fig.3). However, there is still no guarantee at this stage of the game that cloud compensation schemes for retrieving the clear cloumn radiances do not entail a residual error which could introduce a bias of the resulting temperature profiles depending upon the amount and nature of clouds. Such bias, correlated with the weather systems would be very detrimental to the value of satellite soundings. This is why great technological efforts are being made to reduce the impact of cloud contamination either by using a smaller instantaneous field of view or using a different spectral region altogether.

Microwave spectrometry

Now the most radical approach for eliminating the effect of fractional cloudiness and even solid overcast, consists in applying the same remote measurement principle in the microwave part of the earth radiation spectrum, specifically the 60 GH_Z absorption band of molecular oxygen (about 5 mm wavelength).

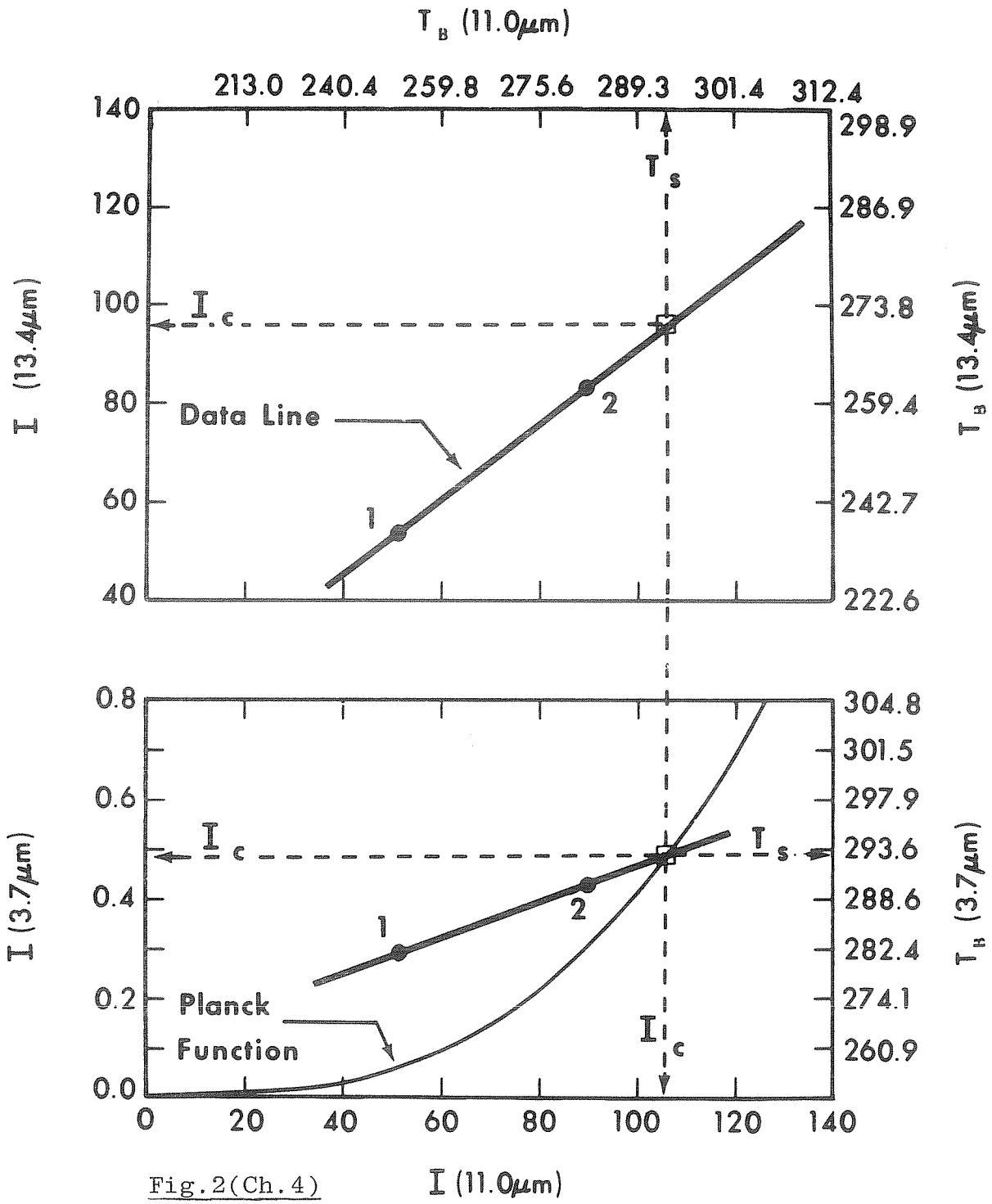

Fig.2(Ch.4)

Determination of the limiting "clear column" radiance using the redundant information of 11μm and 3.7μm atmosphere window channels.

Temperature profile retrieved in partially cloudy atmosphere

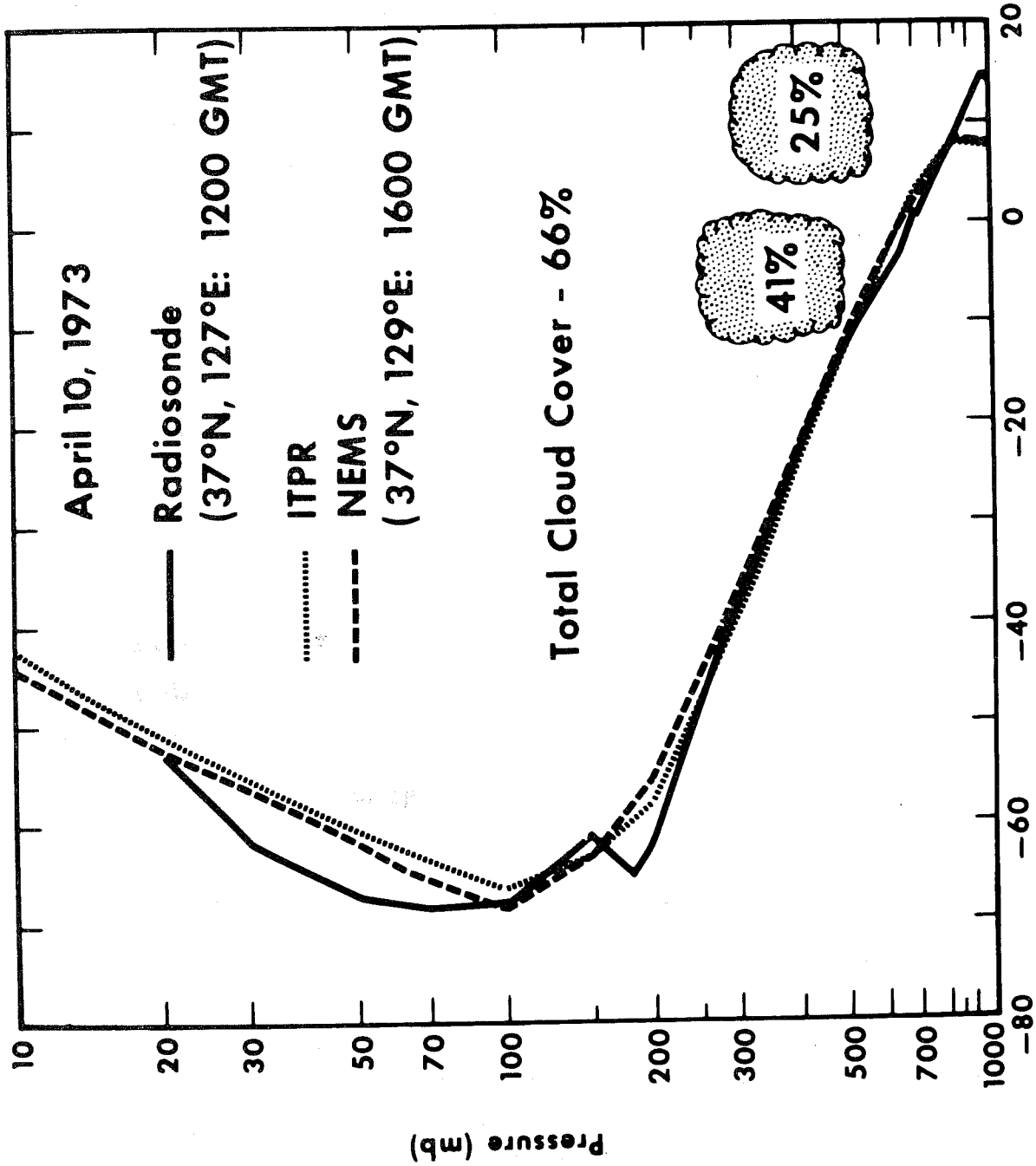

Fig.3 (Ch.4)

The first microwave spectrometer was developed for the Nimbus 5 spacecraft; it incorporated three sounding channels at 53.65, 54.9 and 58.8 GH_Z plus two microwave window channels at 22 and 31 GH_Z. Clouds do not alter the 54.9 and 58.8 GH_Z radiances and only infrequently affect the lower-peaking channel at 53.65 GH_Z where a maximum attenuation of 3K (equivalent brightness temperature) has been observed, consistent with theoretical considerations which show less than a 3K attenuation by a nimbostratus cloud having 0.1 g/cm^2 of liquid water. Clouds which may have a larger water content do not fill the entire 200 km field of view of the radiometer so that their effect is smaller. Because of their remarkable insensitivity to cloudiness,microwave spectral measurements are a precious complement to infrared radiances. But they can hardly be used alone because they lack the relatively good vertical resolution of infrared radiance-data near the surface. A microwave spectrometer will be incorporated in the next generation of operational meteorological satellite in time for the First GARP Global Experiment, and it has been agreed that the expected improvements eventually removes the necessity to complement satellite soundings by a large number of in situ measurements in the persistently cloudy areas such as the 40-50° south latitude belt.

The problem of low level temperature inversion

Even though the peaks of the 15μm radiation weighting functions become sharper at lower altitudes, 15μm radiance data still do not provide adequate vertical resolution near the surface for resolving the often sharp temperature structures at the top of the planetary

boundary layer. A significant step has been made towards solving this problem by including additional sounding channels using the 4.3μm emission band of CO_2. Because the temperature dependence of the Planck function near normal surface temperatures is much sharper at 4.3μm than near the maximum of the longwave radiation spectrum at 15μm, sharper weighting functions obtain in the lower strata of the atmosphere (Fig.4) thus allowing a definitely sharper reconstruction of the lower altitude features of the profile (Fig.5) and corresponding reduction of the residual errors. This improvement tested on Nimbus-6 will also be incorporated in the next generation operational meteorological satellite system.

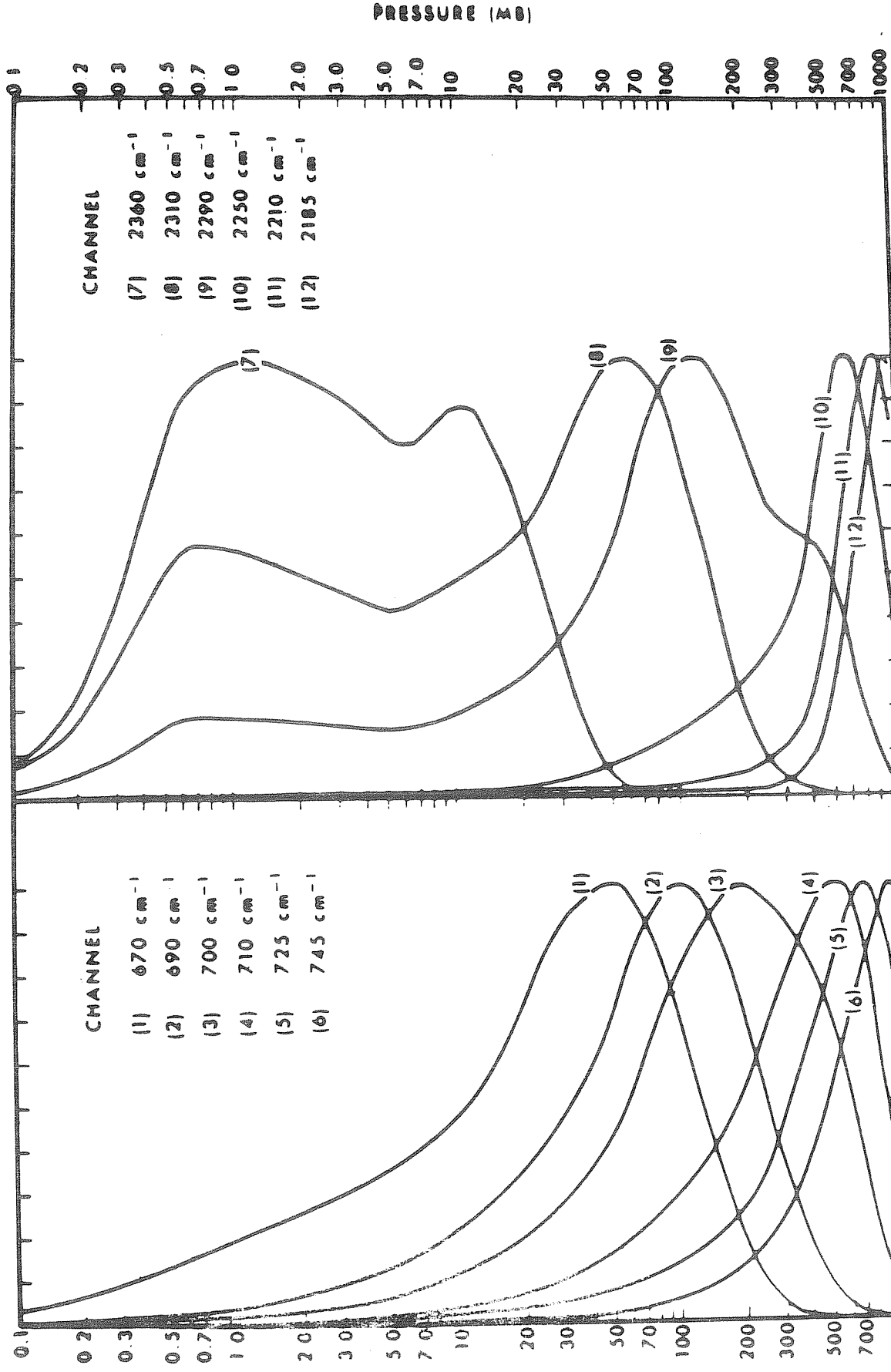

Fig.4(Ch.4)

Weighting functions for the 15 μm and 4.3 μm emission bands of CO_2 (Nimbus-6)

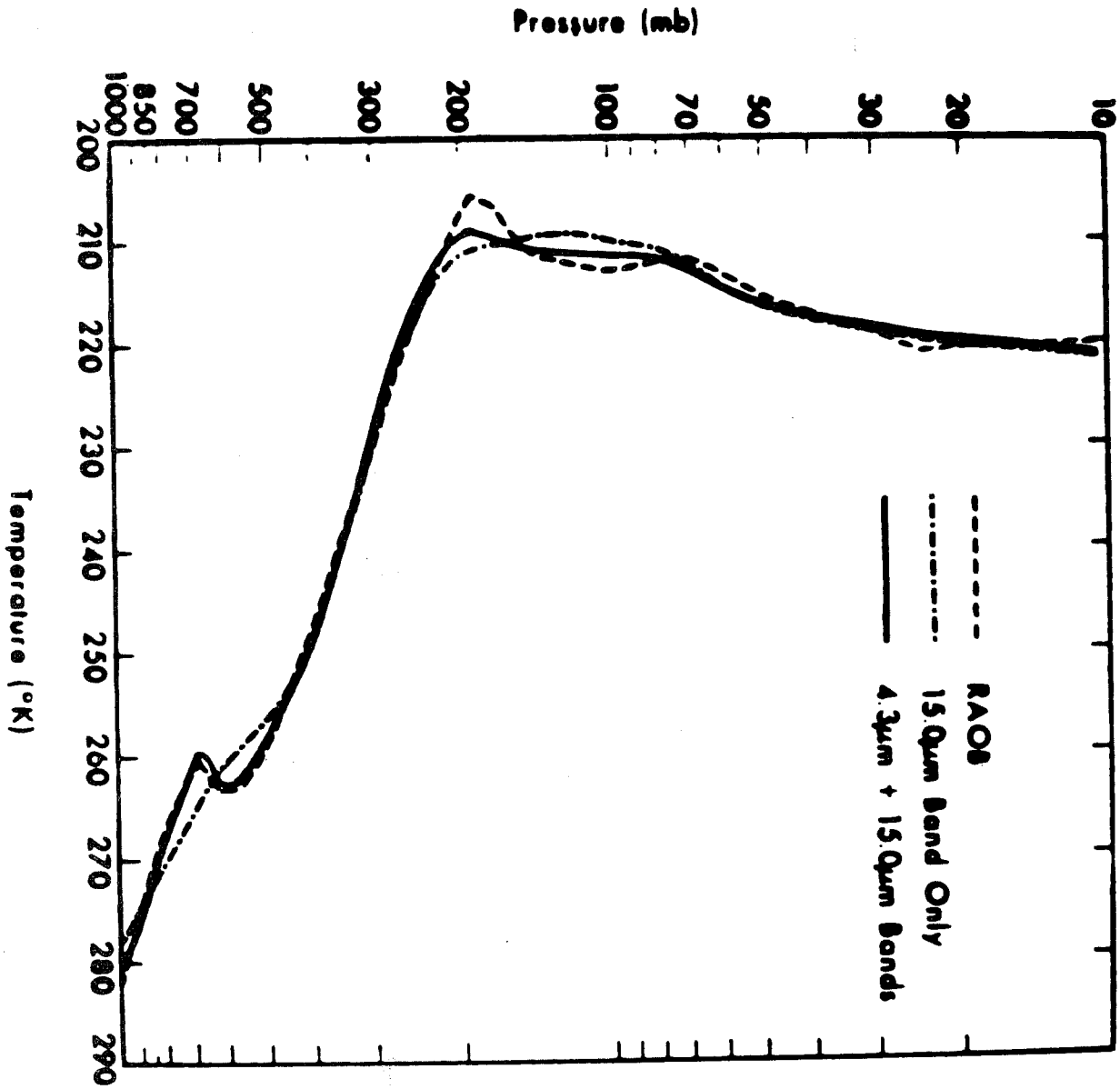

Temperature profile obtained from the inversion of both 15 μm and 4.3 μm spectral data.

Fig.5 (Ch .4)

5. Wind Determination from Cloud Tracers : PART I:

Time lapse photographs of cloud fields taken from the Earth indicate a large variety of motions or deformations superimposed on the mean drift associated with the large-scale wind. Under favorable conditions, e.g. not very active cloud or small vertical shear, the mean drift of cloud ensembles can be very nearly representative of the air flow in which they develop. Under not so favorable conditions, obviously, the apparent mean motion of cloud ensembles or even single clouds may be quite different from the air flow : an excellent example of this situation is given by stationary lenticular clouds associated with a mountain-locked lee-wave.

Professor Suomi of the University of Wisconsin demonstrated in 1966, with his spin scan camera mounted on the geostationary satellite ATS-1, that time lapse photographs taken from a stationary position in space (relative to the Earth) could be obtained with enough accuracy to provide a measurement of the apparent motion of the cloud ensembles. The nature of the motion is illustrated by a large variety of short endless film loops, each showing a sequence of some 30-40 images taken at about 30 minute intervals from dawn to sunset over the disc of the Earth seen from ATS-1 and later ATS-3 (colour pictures). More elaborate productions may show in more detail the development and propagation of cloud patterns associated with meso-scale meteorological systems. Still other films now being prepared with the infrared images obtained by the second generation stationary

meteorological satellites SMS-1 and 2 show continuously the evolution of cloud patterns through day and night. Despite the strikingly high spatial definition displayed on the full disc images : 3000 lines for ATS-1, about 15,000 lines for SMS-1 visible light pictures, individual clouds are not usually resolved. In any case, the time interval of about 30 minutes between successive images is long compared to the lifecycle of an individual cloud so that the smallest details on the cloud field seen on one very high resolution SMS image cannot be recognized on the subsequent image. Thus the correlation of cloud patterns on several time lapse images,spanning a period of 1/2 to 2 hours, is actually based on tracing moderately weak but persistent meso-scale perturbations of the mean flow and the cloudiness associated with such perturbations. The most appropriate size of image samples used for tracing such cloud patterns seems (from the experience of ATS and SMS data) to be 40 to 80 km with spatial resolution of 2-3 km.

The technical problem of tracing and measuring the apparent displacement of a recognizable cloud pattern on time lapse photographs is two-fold. One must first determine the correspondence between the coordinates of one particular geographical location on one image with its coordinates on the next image, with due account for image distorsion, rotation and/or x-y shifts associated with residual spacecraft motions away from the ideal (nominal) stationary position and attitude. This is generally referred to as the navigation problem. Secondly, one must associate a set of x-y coordinates to a more or less shapeless pattern of cloudiness on one image and recognize the x-y position of the most similar pattern on subsequent images : this is the tracking problem.

The navigation problem

If a geostationary satellite were in a perfect orbit, every picture taken could be overlayed on the others without any discrepancy of the Earth landmarks. However, because ATS and SMS satellites are not in perfect orbits, the Earth moves in the frame. This false motion is due to the satellite's motion. Navigation is the process of removing the satellite's motion from the cloud motion computation or alternately, the process of establishing the one-to-one correspondence between image coordinates determined by the instantaneous geometry of the Earth, satellite and scanning telescope axis on the one hand, and fixed Earth coordinates on the other hand. This is a classical problem of space dynamics and a difficult one at that,considering the exacting accuracy requirement of this particular mission : 1 km at a distance of 36,000 km is only 6 arc-seconds. But the solution is greatly helped in the case of a spinning spacecraft by the gyroscopic rigidity of a frictionless spinning body. This gyroscopic attitude stabilization affords a long "memory" of many hours during which the slow drift of orbital and satellite attitude parameters may be monitored at leisure without interference from either station keeping or attitude control corrections. Thus navigational data are obtained by using the most precise information available, i.e. the high resolution image itself and tracking the apparent motion (in image coordinates) of several landmarks adequately distributed on the disc of the Earth. Except for a consideration of the specific contrast of landmarks (requiring specific contrast enhancement techniques), the technical

problem of tracking apparent landmark motions is quite the same as tracking cloud patterns except that landmarks do not deform but may be somewhat obscured by overlying cloudiness. Extremely precise navigation yielding residual errors well under the size of one picture element (1 km x 1 km) is now possible with second generation geostationary satellites like SMS or the European Space Agency METEOSAT.

In a recent exercise with SMS image data performed by the University of Wisconsin group during the January 1975 Data Systems Test in the United States, navigation based on modeling the orbit and attitude motions of the spacecraft explicitly (dynamical model) yielded RMS residuals of 0.135 m sec^{-1} for the zonal component of the wind and 0.10 m sec^{-1} for the meridional component. This corresponds to an average navigation error in the east-west direction of only 243 m between two images taken 30 minutes apart, and 184 m in the north-south direction. The largest residual was 0.38 m sec^{-1} in the u component which corresponds to a 685 m navigational error. This is to be compared to the visible pixel size of approximately 800 m. Consequently, navigation errors and misalignment of the images are definitely smaller than one visible pixel, even when using infrared data which has a spatial resolution four times as large as the visible.

Cloud tracking

Tracking of cloud patterns may be done by either of two primary methods : visual tracking of a cloud element on a sequence of images using the cinematographic impression provided by such "movies" or matching corresponding samples of two successive images in order to find the best possible correlation between the two.

The visual method or "movie loop" method is historically the first one applied operationally by the National Environmental Satellite Service (NOAA). The technique is now refined by using a television display of the relevant image samples shown in quick succession and aided by displaying a cursor which can be adjusted to match any detail to the nearest TV line and element (pixel tracking) without losing any of the original geometrical information of the image (the very rich multispectral contrast information contained in the original data cannot be displayed on a television scope). This method may be quite accurate, depending upon the operator's skill and the time available for analysing one image sector. Excellent results have been obtained in a research environment ($\pm$ 1 pixel accuracy); the visual method may thus be preferred for use by students and/or when the complexity of the 3-dimensional cloud distribution and cloud dynamics requires the attention of a trained analyst.

The correlation method on the other hand is the fastest and most accurate technique under operational constraints when well defined clouds can be seen moving in a single layer flow pattern.

Note that automatic cloud layer discrimination in complex multi-layer situations may yet be possible by applying various monochromatic or multispectral contrast enhancement schemes : these possibilities have however hardly been explored yet and are subject to further research. Correlation matching of corresponding samples of two successive images provides,under the best circumstances (about 3/4 of cases) a very clearly defined correlation maximum, the position of which gives the most probable relative displacement $\Delta x - \Delta y$ of the cloud patterns with better than 1 pixel accuracy.

Finally then, one will see that the measurement of the apparent displacement of cloudiness, as observed from a geostationary satellite, can be obtained with better than 1 pixel accuracy e.g. about 2-4 km for SMS visible or 5 km for METEOSAT infrared images, thus yielding an instrumental error well under 1 m sec^{-1} for time lapse sequences extending over a 1 hour period. This instrumental error estimate is not however the whole story when it comes to inferring a determination of the wind because even if clouds were perfect tracers of the air flow, there is yet no completely satisfactory way to relate one particular cloud pattern to a specific altitude in the 3-dimensional air flow, and because clouds are not exact tracers of the air flow, particularly when a significant vertical shear exists.

Cloud height determination

The variation of wind speed and direction with height can be quite large. Consequently, the accurate determination of the

height of the cloud being tracked is important. This in effect can be one of the major causes for errors in the computation of winds from cloud motions. There are several ways in which cloud heights can be determined. In the absence of any other information but visible images such as given by ATS, an experienced analyst can make an educated guess about cloud altitudes by identifying the cloud type, e.g. cirrus or trade-wind cumulus etc... This approach has been shown to allow discriminating two levels : one "low level" about 900 mb and one high level about the tropopause.

Another method of determining cloud heights consists in using stereographic image pairs obtained with overlapping photographs from one single orbiting spacecraft or two different spacecrafts. In any case, the height resolution is limited by the pixel size on the image and the baseline for stereographic viewing. Thus, this purely geometric approach holds promise of the best vertical resolution and absolute accuracy, up to 10-20 levels. On the other hand, the method is still under development and has never been implemented so far in conjunction with cloud tracking.

Still another method for determining cloud heights is based on using multispectral radiometric data. If a single layer of cloudiness is apparent in the field of view of the radiometer - spectrometer, the (fractional) amount of clouds and their altitude is a by-product of the process of inversion of satellite sounder data. A vertical resolution of 10 levels is possible but the method has never been implemented so far because temperature

sounding information come in a quite different data stream than that of geostationary satellites. This situation will be changed with the next series of SMS carrying the experimental "Vertical Atmospheric Sounder" radiometer.

In actual practice, the cloud height is presently determined from a simultaneous analysis of both visible and thermal infrared images transmitted by geostationary satellites. The main problem with this method is that clouds are not necessarily opaque black body radiators so that part of the energy reaching the sensor comes from the surface through the cloud layer, thus making the clouds appear warmer than they actually are. There is a need,therefore, to determine the optical thickness of the cloud from its visible brightness. The optical thickness is then used to estimate the infrared emissivity. This value of the IR and the fractional cloud cover determined also from the visible image, are used to correct the black body temperature. Obviously, this process can only be applied during the day. The accuracy of the scheme has not been fully established but is estimated to be equivalent to about 10 vertical levels. The largest sources of errors in this system appear to be the fractional cloud cover determination, and the variance in scattering caused by the finite shapes of clouds not accounted for by the multiple scattering model in the system.

Errors in the height computation can also be caused by several factors, in addition to the basic limitations of the system. If there are thin cirrus (or "invisible" cirrus) over lower clouds, the system may track the motion of lower clouds, but actually

measure the height of the upper clouds, thus assigning the motions of lower clouds to the wrong altitude. The reverse error may also occur when the system tracks a hole in an otherwise homogeneous layer of thick upper clouds. A high temperature and correspondingly low altitude, would be wrongly assigned to the velocity reading. Another source of error in the height computation is the fact that the system measures the cloud top temperature while the cloud drift correlates best with the mean velocity in the entire cloud layer (cirrus) or the wind at cloud base (cumulus).

Indeed, extensive intercomparison tests carried out in the Tropics with satellite as well as aerial observations of clouds, and in situ wind measurements using instrumented aircrafts with inertial guidance, showed that the displacement of the trade-wind cumuli correlates extremely well ($\pm$ 1 m/sec) with the wind velocity at the cloud base, i.e. about 100 meters above the lifting condensation level. Since this level varies very little in the course of time, a very precise altitude coordinate, known from climatology, can be associated with "low level" cloud measurements in the trade-wind regions.

Clouds not moving with the speed of the wind

Not all apparent motions discernible on a satellite picture sequence can be attributed to clouds drifting with the wind. Apparent motions can be caused by growth and dissipation of cloud systems. Fujita et al. (1975) have shown that cloud type and size influence growth and dissipation which in turn limit the accuracy of a cloud wind measurement. Fog dissipation is another

obvious example of "false" cloud motion. Orographic effects such as caused by mountains are also obvious exceptions : the wind blows past the mountain, but the cloud pattern remains stationary in the lee of the mountain. Another remarkable exception is associated with the propagation of gravity waves. Gravity waves which form on density discontinuities in the atmosphere do not move with the wind at that level, therefore, tracking clouds produced by the gravity waves may introduce large errors. Gravity waves can be a severe problem for cloud tracked winds in the vicinity of jet cores or strong inversions. Other motions of clouds which are not directly related to the wind can be caused by frontal and large-scale wave propagation. The large-scale motion of an upper air trough, and the weather associated with it, do not move with the same speed and direction as the wind. Careless tracking of these features will produce the velocity of the disturbance, not the velocity of the wind.

But the reader should not hasten and draw the conclusion that satellite wind data from tracking cloud motions, are beset by so many instrumental and physical difficulties as to be essentially useless. The second generation geostationary satellites (SMS) have been in operation only one year and it has already become apparent that continuous surveillance of the development and decay of weather systems from such privileged vantage points provides a vast amount of information which may require a great amount of thoughtful analysis but will not be matched for spatial resolution by any ground based system.

6. Wind Determination from Cloud Tracers : PART II:

The quality of satellite wind data, compared to radiosondes and/or detailed in-situ measurements of the wind velocity, is still a controversial question and, in fact, quite naturally so as the state of the art is evolving rapidly.

The first and most straightforward means to "verify" this new wind measurement technique consists in comparing its results with the well-established radiosonde wind observations obtained at nearly the same times and locations. A typical application of this verification approach is illustrated in Fig.1 which exemplifies one particular set of low level winds inferred from SMS-1 cloud images over the B-scale network of the GARP Atlantic Tropical Experiment. Thin arrows indicate satellite winds and full arrows nearly simultaneous radar wind measurements. A detailed study indicates an obvious general agreement between both types of data but also points out one difficulty caused by the very real variability of the wind field on the smallest spatial scales which are resolved by the cloud wind data but not by the much coarser radiosonde network. This spatial variability may account for a large fraction of the discrepancies found between not exactly coincident wind observations of the same kind (radiowind-radiowind comparisons) as much as observations of different kinds (radiowind-cloud wind comparisons).

Reproducibility tests

A considerable effort was conducted recently by the University of Wisconsin group to extract about 1000 wind determina-

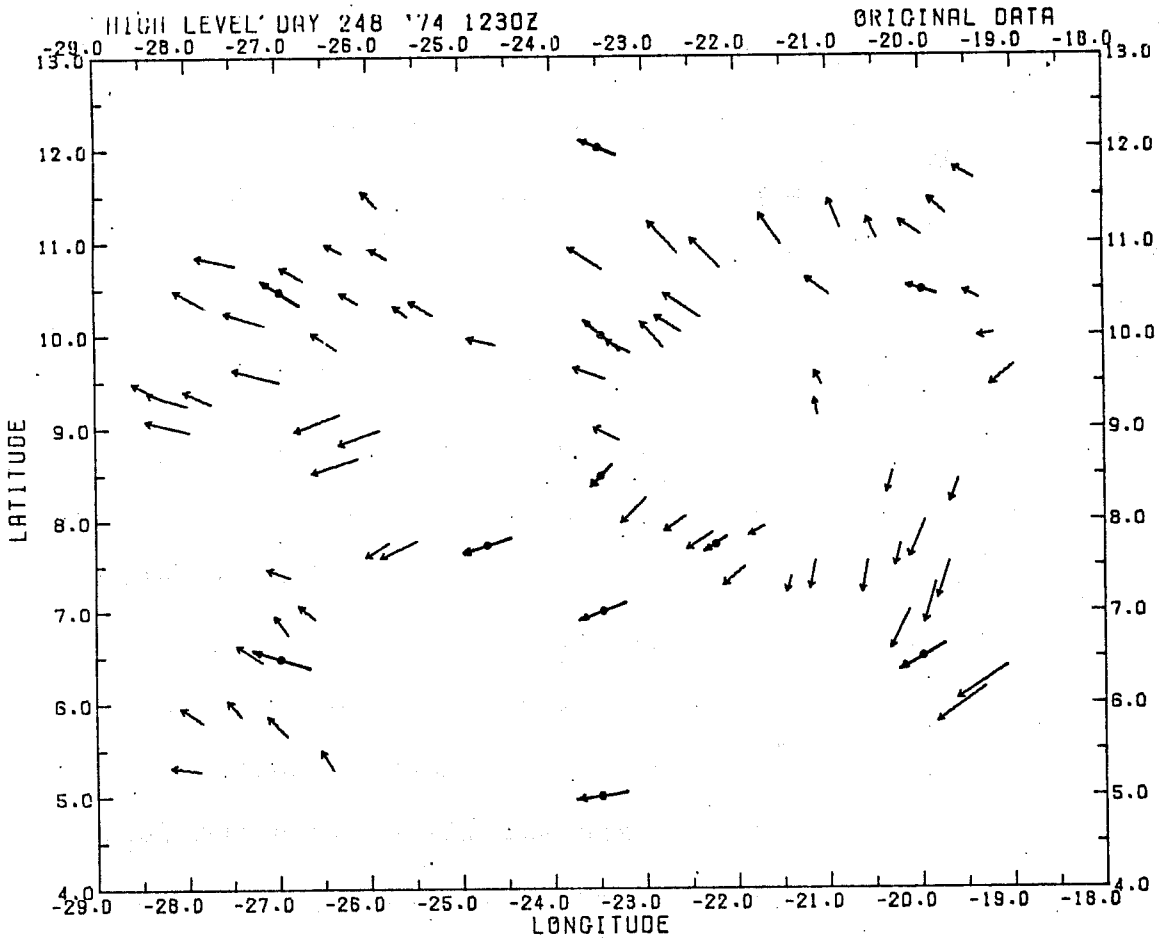

Fig.1: (Ch.6/II)

Typical example of high level winds determined from cirrus cloud motions measured over the GATE area. Thick arrows are ship radar wind measurements at 200 mb.

tions per day from SMS full disc cloud images during the recent Data Systems Test. Because the man-machine interactive process used in this test did involve moderately experienced meteorologists (graduate students) to a considerable extent, a reproducibility exercise was carried out in order to test how reliably could different operators measure the wind velocity from the same cloud image data. In this test, low level cumulus (about 950 mb) and cirrus clouds (about 200 mb) were tracked manually; six different operators produced their own wind data sets independently. These raw wind sets underwent objective analysis to obtain grid point values of the u- and v-components of the velocity, and the grid values of the divergence and vorticity. A total of ten randomly chosen intercomparison sets were made in overlapping valid data regions (where appropriate clouds could be tracked), after editing out the largest discrepancies when based on one questionable determination. The reproducibility statistics were as follows :

	Low level winds	High level winds
$\bar{u}$	3.2 m/sec	8.56 m/sec
RMS Δu	0.8	1.7
$\bar{v}$	5.25	2 [illegible]
RMS Δv	1.3	1.1

These statistics are therefore consistent with a 2 m/sec limit for the reproducibility of total wind velocity at cirrus level, and 1.3 m/sec at cumulus level : this can be considered as the most significant "instrumental" noise error introduced by the process of extracting wind velocity data from satellite pictures, in addition to possible physical errors associated to insufficient

sampling of the vertical structure of the wind field and uncertainty about the cloud altitudes. The higher level of agreement between cloud wind determinations at the lower altitude can be attributed to the larger number of tracers at that level, as well as to the distinct appearance of tradewind cumuli contrasted to the amorphous character of cirrus clouds. A further indication of the internal consistency of cloud winds can be derived from estimates of the vorticity and divergence fields. Reproducibility statistics for these derived fields were as follows:

	Low level	High level
Vorticity	3×10^{-5} sec^{-1}	4×10^{-5} sec^{-1}
Mean discrepancy	10^{-5}	10^{-5}
Divergence	8.6×10^{-5} sec^{-1}	7.7×10^{-5}
Mean discrepancy	1.1×10^{-5}	1.6×10^{-5}

In every case studied over the GATE area, the dominant features of the mesoscale wind field defined by conventional measurements, were also present in the cloud wind field. In every case, the cloud wind field shows more structure than the ship-based network, as expected from the potentially much finer spatial resolution of the former; this structure is consistent with major cloud patterns and also evolves in consecutive wind sets in accord with the meteorological pattern.

Cloud tracers versus rawinsonde comparison

A recent test of this nature has been conducted with about 14 000 cloud wind determinations obtained during a 14-day period in the winter 1975, using three visible SMS images for cloud

tracking and a single infrared image for computing the cloud temperature and height. Because the cloud winds measured at about 18 Z are not coincident in space nor in time with any conventional upper air measurements, a time and space interpolation program was written and applied to each cloud tracer wind determination. This program searched for the 3 closest (within a 660 km radius) radiosonde reports for both 0 Z and 12 Z reporting hours bracketing the cloud wind report time, and interpolated these upper air measurements to the location and time of the cloud wind to produce statistics of the cloud versus rawinsonde wind differences. Similarly, the same (space only) interpolation scheme was applied to rawinsonde data only to produce statistics of radiosonde versus radiosonde wind differences under the same conditions. The mean distance to the nearest rawinsonde station was about 300 km in both cases. The statistics for all cloud types and cloud heights mixed, are as follows:

	Cloud vs. rawinsonde	Rawinsonde vs. rawinsonde
RMS u difference at same level	5.5 m/sec	5.1 m/sec
RMS v difference at same level	4.5 m/sec	4.3 m/sec

These rather large discrepancies were previously thought to be attributable to the vertical wind shear and large errors in fixing the cloud tracer altitudes. Thus, for the purpose of compensating for this particular cause of error, it had been proposed to compare the cloud winds with radiosonde winds at the level where they would best fit. Statistics for comparison at

this "level of best fit" did not indicate a clearer distinction between both type of data:

	Cloud vs. rawinsonde	Rawinsonde vs. rawinsonde
RMS u difference at level of best fit	2 m/sec	2.6 m/sec
RMS v difference at level of best fit	2.3 m/sec	2.8 m/sec

Thus ,the major cause for large discrepancies in this kind of verification studies must be associated with horizontal rather than vertical wind shear. One could therefore conclude from such statistics that carefully produced cloud tracer winds do not materially differ from radiosonde wind measurements at about the same level . It should be remembered at this point that wind determinations obtained by tracking a rising balloon are far from perfect,as RMS wind vector errors determined for a current radiowind set (compared to high accuracy rocket tracking radar) is 1-3 m/sec for light winds and up to 10-20 m/sec at cirrus level for moderate to high winds.

It must be clear then that cloud winds versus radiosonde winds comparison cannot in itself determine the accuracy of the former. The analysis quoted here showed the same average differences of about 5 m sec^{-1} for each u- and v-components between cloud and radiosonde winds, or between radiosonde winds themselves. Studies of atmospheric variability also predicts this order of magnitude of differences for point measurements and the analysed (smoothed) wind field : see for example fig.2.

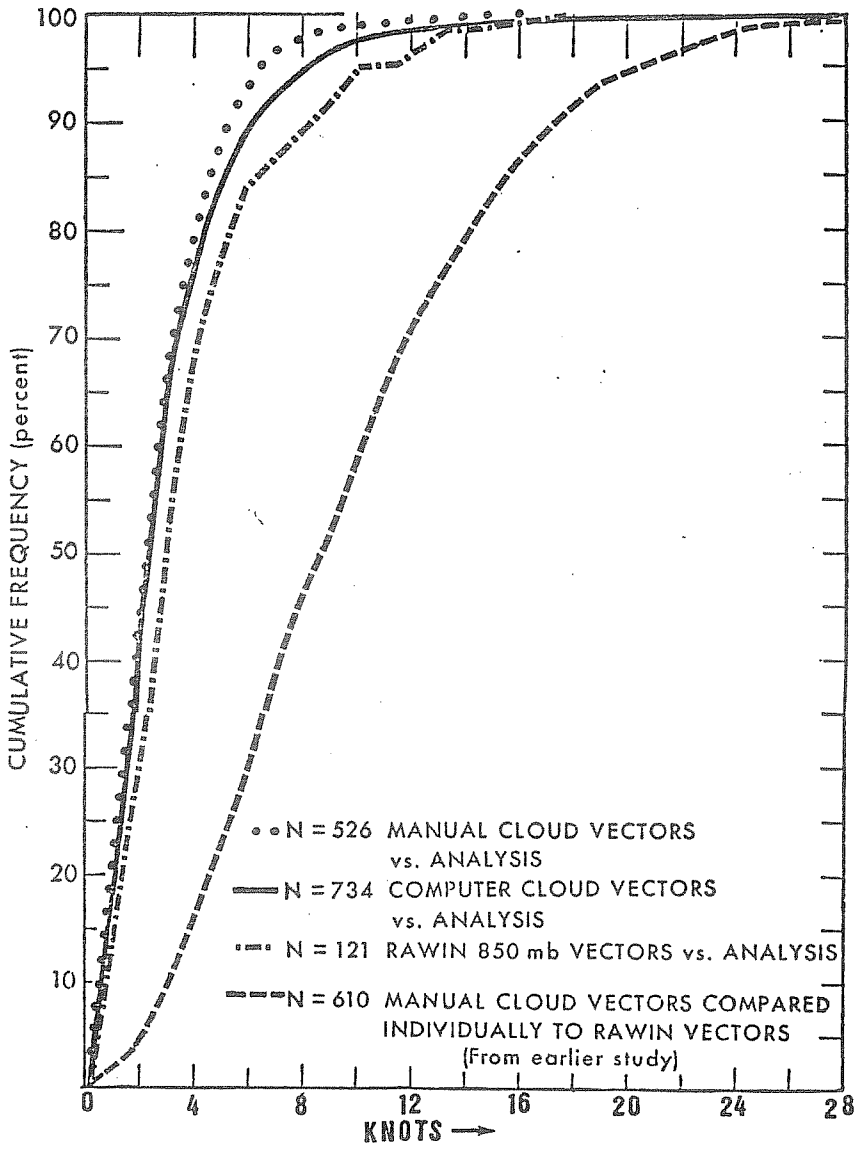

Fig. 2: (Ch.6/II)

Statistics of vector differences between cloud winds and conventional radiowinds, or same with the analysed wind field. Note the much larger differences between individually compared point measurements, as expected from atmospheric variability.

Direct comparison with in-situ aircraft measurements

The direct comparison of cloud tracer winds with ground truth winds would appear to be the most effective method for establishing satellite wind quality at the exact time, location and altitude of the wind determination. This method is unfortunately rather expensive as it involves flying instrumented aircrafts at various levels and using very precise navigation techniques for determining the aircraft trajectories with an accuracy well within 1 m/sec. A verification experiment of this nature is in progress under the guidance of Hasler and Shenk at the Goddard Space Flight Center. One or more low level instrumented aircrafts, equipped with an Inertial Navigation System (INS) are flown to define the vertical extent and horizontal motion of selected clouds at various altitudes within the cloud field, and also to measure the vertical structure of the ambient wind field. One high level photographic plane also used with INS is used to describe the horizontal structure of the cloud field and to measure its apparent motion. The aerial photographs are also used to identify in the satellite picture,the selected clouds observed by the low level aircraft or aircrafts. As of today, these experiments have been conducted over the tropical ocean off the coast of the United States and Mexico only. A total of 40 tropical cumulus clouds and 5 cirrus clouds have been tracked.

As could be expected, the best agreement was found for low level cumulus cloud motion compared with the wind velocity measured at cloud base level. The RMS vector difference between the aircraft measured cloud motion and the actual wind at cloud base is

1.3 m/sec for cases with track lengths of 1 hour or longer. But the agreement with the "surface wind" measured on very low altitude aircraft runs (150 m) is not significantly deteriorated : RMS vector difference about 1.6 m/sec. On the other hand, cloud motions do not fit well the wind at cloud top level. One should emphasize that navigational and cloud tracking errors in these experiments are of the order of 1 to 1.5 m/sec so that the fit of low level cloud motions with the cloud base wind must be essentially exact. This affords therefore a very accurate determination of the altitude of best fit (about 950 mb) for low level cloud winds derived from satellite observations.

Much larger vector differences were found however in the few cases of cirrus clouds. Mean vector differences of 3.6 m/sec (respectively 7 m/sec) obtained between the aircraft measured cloud motion and the wind at mid-cloud level (respectively cloud top level). Indeed, the cirrus motion speeds agreed best with the mean wind in the whole cloud layer with a residual vector difference of about 2 m/sec. This indicates that cirrus clouds may not be good tracers of the wind at any one level in their range of altitude (as determined by point measurements) but may still provide a very useful indication of the mean wind in a moderately thick layer, i.e. a kind of data most germane to the application in general circulation models.

Conclusion

I would like to conclude from this that surely the last word has not been said about how accurate, how useful and how homogeneously distributed are cloud tracer wind data determined from geostationary satellites. There are tentative and indeed sketchy indications that cloud tracers could provide, under appropriate circumstances, very accurate wind estimates, within 1-2 m/sec. One knows also examples of much larger discrepancies being repeatedly quoted in the literature and often wrongly interpreted as "errors" while overlooking the specific deficiencies of in-situ measurement techniques and very real sampling errors due to the large atmospheric variability over distances like one GARP grid (see Great Britain Met. Office 1940; Arnold, 1955). We may expect that the development of the FGGE array of five geostationary satellites and concurrent progress of wind extraction techniques will help resolve these differences of views and also, more significantly, the physical discrepancies in this global wind measurement system.

REFERENCES

1 - ARNOLD : Representative winds aloft.
Bull. Am. Meteor. Soc., 37, 27-30, 1965.

2 - FUJITA, PEARL and SHENK : Satellite-tracked cumulus velocities.
J. Applied Meteor., 14, 407-413, 1975.

3 - Great Britain Meteorological Office : Variations of wind with distance and time.
Meteor. Office Monograph 389, 1940.

4 - HASLER, SHENK and SKILLMAN : Wind estimates from cloud motions.
To be published in J. Applied Meteor. 1975.

7. Space-Time Structure of Meteorological Fields and Objective Analysis

The remarkable, and to a large extent unpredictable (?) variability of meteorological parameters has inspired many authors to look up the theory of random variables for a cue on how best reconstruct one particular realization of these meteorological fields on the basis of (possibly a small number of) discrete measurements. Gandin (1963) was the first to suggest a truly consistent application of statistical knowledge regarding the space structure of the meteorological fields at one single time to the problem of objective analysis. Gandin's ideas are as follows. Consider one particular meteorological field $f(x,t)$ which is to be determined at one particular time t using all a priori knowledge, e.g. climatological records and even forecasts from the previous days, plus some instantaneous discrete measurements $f_i = f(x_i,t)$ at stations x_i and time t. Now, because of the known correlation between the value of parameter f at one place x_i and that at nearby locations x_j, it is unlikely that this particular field should exhibit a discontinuity or even a sharp gradient in the vicinity of the stations x_i. Thus, it should be possible to estimate the (most probable) value of the meteorological field in the vicinity of the stations x_i by an appropriate smoothing operator which will be chosen, for algebraic convenience, a linear combination of the observation. Let then $f^o = f^o(x,t)$ be a first guess of the meteorological field under consideration at time t, e.g. the climatological mean value of field $\bar{f}$ or a simple persistence forecast f^{-1} since the previous day or any

combination of both. Observed values f_i stations x_i can be expressed in terms of this first guess plus an observed derivation f'_i, thus:

$$f_i = f^o_i + f'_i \tag{1}$$

The true (but unknown) value of the field at one location of interest, e.g. one particular grid point, may be expressed similarly:

$$f = f^o + f' \tag{2}$$

We shall study the possibly of <u>estimating</u> f by replacing f' by a linear combination of the observed f'_i at surrounding stations:

$$f \approx f^o + \sum_i p_i f'_i \tag{3}$$

where the weight coefficients p_i of the linear combination are chosen so as to <u>minimize in a statistical sense</u> (but not necessarily for one particular realization) the error:

$$d = f - (f_o + \sum_i p_i f'_i) \tag{4}$$

A reasonable optimization criterion is that the mean square error $\overline{d^2}$ be minimum over an ensemble of independent realizations of the field, for one given geometrical configuration of stations and grid point x. Thus:

$$\overline{d^2} = \overline{f'^2} - 2\Sigma p_i \overline{f'f'_i} + \Sigma\Sigma p_i p_j \overline{f'_i f'_j} \tag{5}$$

Differentiating with respect to each coefficient p_i and setting the result equal to zero yields the following set of equations:

$$\overline{f'f'_i} - \Sigma p_j \overline{f'_i f'_j} = 0 \tag{6}$$

which involves the covariance of the field at various locations x, x_i, x_j, ... Now let σ_o, σ_i, σ_j be the variances of the meteorological field at these locations and μ_{oi}, μo_j, μ_{ij} the

correlation coefficients:

$$\mu_{ij} = \frac{\overline{f'_i f'_j}}{\sigma_i \sigma_j}$$

Let us also assume (for simplicity) that the field is statistically homogeneous so that μ_{ij} is essentially a function of the vector distance:

$$r_{ij} = x_j - x_i$$

and the variances σ_o, σ_i, σ_j are approximately the same. The system of equations (6) then read:

$$\sum_j \mu_{ij} p_j = \mu_{oi} \qquad (7)$$

Space correlation properties of meteorological fields

For obvious practical reasons, much attention has been given by practising meteorologists to the problem of establishing the correlation range, and generally, the significance area of the various meteorological parameters. Covariance and correlation data compiled by many authors are available in the literature. We shall quote only one recent study involving 50 stations over the continental United States (Fig.1) by Schlatter (1974). It turns out that correlation coefficient estimates for geopotential height are approximately isotropic (Fig.2) and fit approximately a gaussian curve like:

$$\mu_{ij} = A \exp(-Br^2) \qquad (8)$$

where r is the distance between stations x_i and x_j and A, B are coefficient which depend upon the nature of the first guess.

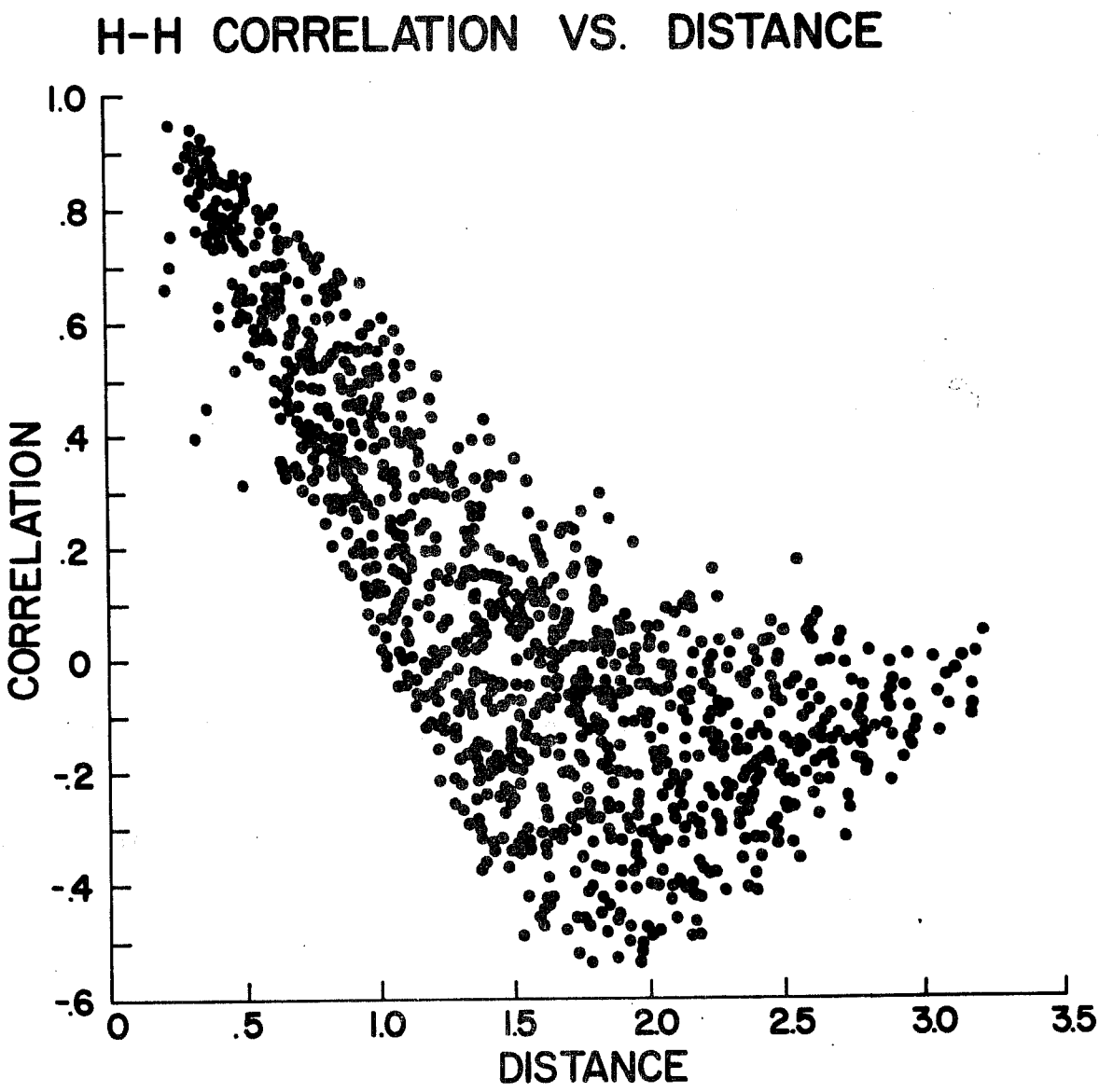

Fig.1 (Ch.7) Correlation of deviations of 500 mb geopotential height from a damped persistence forecast for every pair of continental U.S. radiosonde stations.

For the 500 mb geopotential height field and r expressed in units of 1000 km, Schlatter's study yielded:

First Guess	A	B
Climatology	0.99	0.6
Persistence	0.93	1.2

meaning that the correlation range for 500 mb geopotential height data is about 1300 km for deviations from climatological mean but only 900 km if one is considering deviations from a persistence forecast. Note that deviations from a one day persistence forecast are normally much smaller than deviations from the long term average, and correspondingly more random.

Furthermore, covariance or correlations for other couples of meteorological parameters such as the u and v- components of the wind may be deduced from the h-h correlation law through the approximate geostrophic relation, e.g.:

$$\overline{h'u'_j} = -\frac{g}{f_j}\frac{\partial}{\partial y_j}(\overline{h'_i h'_j})$$

$$\overline{u'_i u'_j} = \frac{g^2}{f_i f_j}\frac{\partial}{\partial y_i}\frac{\partial}{\partial y_i}(\overline{h'_i h'_j})$$

$$\overline{v'_i v'_j} = \frac{g^2}{f_i f_j}\frac{\partial}{\partial x_i}\frac{\partial}{\partial x_j}(\overline{h'_i h'_j})$$

and so forth. Thus, even if the correlation functions for pressure or geopotential height is essentially isotropic, the corresponding geostrophic wind correlations isolines are definitely <u>not isotropic</u> and stretched in the direction of the wind component, e.g. the isolines of correlation for the zonal u-component are stretched in the zonal direction and compressed

Table 5. A sampling of published spatial correlations or covariances based upon daily observations of geopotential height (h), wind (u,v) and temperature (T).

Investigators	Variables	Location	Levels	Month or Season
Alaka and Elvander, 1972	h, u, v, T	Caribbean	850, 500, 200 mb	January, July
Bertoni and Lund, 1963	h	Europe	sea level, 850, 700, 500 300, 200, 100 mb	Winter
Boltenkov, 1966	T	U.S.S.R.	1000, 850, 700, 500, 400, 300, 200, 100 mb	Winter
Buell, 1958	h, u, v	U.S.	500 mb	Summer, winter
Buell, 1959	h, u, v, T and all cross-correlations	U.S.	500, 300, 100, 30 mb	Summer, winter
†Buell, 1962	v_ℓ, v_t	U.S.S.R.	300 mb	March
		Europe	700, 500, 300, 200, 100 mb	Winter
		Canadian Arctic	500 mb	Summer
		U.S.	850, 500, 300, 200, 100 mb	Summer, winter
†Buell, 1972a	h, v_ℓ, v_t	North America	500 mb	Summer
Dartt, 1972	u, v	West Central tropical Pacific	700, 500, 250 mb	Summer
Fortus, 1964	h	U.S.S.R.	850, 700, 500, 300 mb	Winter
Gandin, 1963	sea-level pressure	Northwest Europe Western U.S.S.R.	Sea level	Winter
Gandin and Kuznetsova, 1965	h	Europe and western U.S.S.R	850, 700, 500, 00 200 mb	Winter
Petersen and Truske, 1970	h, u, v, T	Caribbean	500 mb	January
		U.S.	500 mb	January
Ramanathan, Y. et al., 1973	u, v	India	500 mb	Winter

†v_ℓ and v_t refer to components of the wind resolved along the line joining the two points (longitudinal component) and normal to that line (transverse component)

in the other direction. Also, since zonal and meridional components correlations are derivatives of the height-height correlation, their correlation range is usually shorter. For the u-component, the correlation range would be the same as that of geopotential height in the zonal direction only but about half as long in the meridional direction. The converse applies to the v-components, obviously (Fig.3 and 4). These correlation properties are well confirmed by experimental studies, notably by the USSR Hydrometeorological Service (space and time correlation vary with latitude, however).

Computing the optimal weight coefficients

For any particular configuration of the location x and the N observing stations x_i, the most appropriate weights p_i must be found by resolving the system of N independent linear equations (7), where μ_{ij} are coefficients to be determined from local statistics or extrapolated from correlation studies published in the literature. It turns out that the main property of the algorithm is to provide appropriately reduced weight to "redundant" observations separated by a short distance compared to the correlation range.

Consider for example determining a field value at point x at equal distances from station x_1 and x_2, also using the "redundant" measurement obtained at station x_3 very close to x_1. Thus:

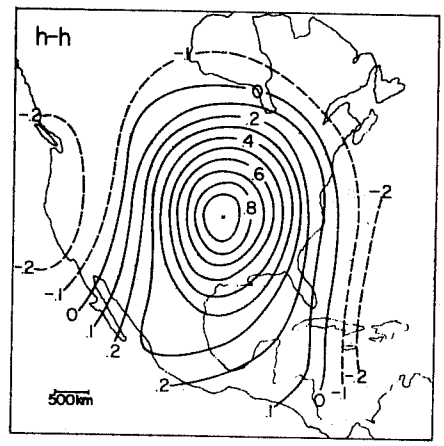

Fig. 2 (Ch.7) Isolines of the covariance of the 500 mb geopotential height over the U.S.

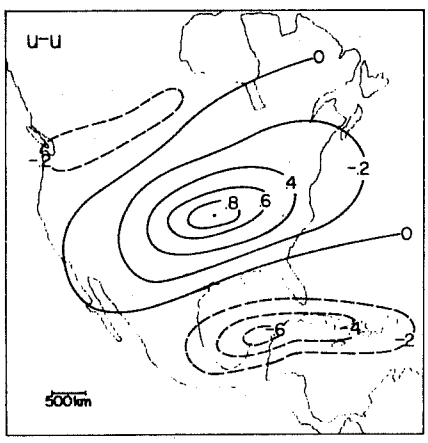

Fig. 3 (Ch.7)

Isolines of the covariance of the u-component of the wind at 500 mb.

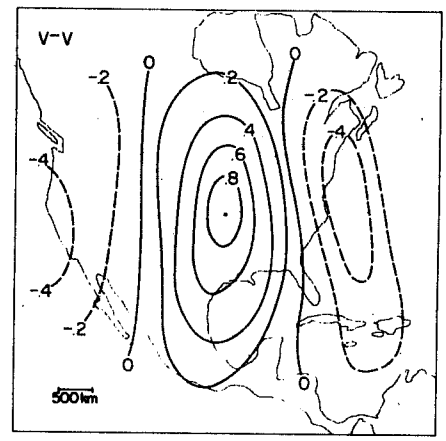

Fig. 4 (Ch.7)

Isolines of the covariance of the v-component of the wind at 500 mb.

$$\mu_{01} = \mu_{02} = \mu_{03} = \mu$$
$$\mu_{13} = \mu_{31} \approx \mu_{11} = 1$$
$$\mu_{12} = \mu_{21} = \mu_{31} = \mu_{13} = \mu^4$$

where use has been made of approximation (8). The linear system reduces then to:

$$p_1 + p_3 + \mu^4 p_2 = \mu$$
$$p_1\mu^4 + p_3\mu^4 + p_2 = \mu$$

or

$$p_1 + p_3 = p_2 = \frac{\mu}{1+\mu^4}$$

is equal to 1 when all correlation coefficients approach 1, but exceeds 1 when $\mu \approx 0.8$. This expresses the statistical fact that if both deviations f'_1 and f'_2 are positive and nothing is known about the field at further distances, it is likely that the deviation should have a maximum between x_1 and x_2. It can be shown that the sum of the weight is equal to 1 or smaller when using a regularly distributed array of discrete measurements.

Multivariate analysis of meteorological fields

Gandin (1963) suggested first, and many authors subsequently applied multivariate statistical analysis schemes to meteorological fields. I shall quote here the latest such results (Schlatter, 1975). The method consists in analysing simultaneously the geopotential height field and the horizontal wind fields (u and v-components), fully taking into account the experimentally determined or computed

correlations between the three variables. One would therefore replace the estimator (3) by a vector expression for:

$$f = \begin{pmatrix} h \\ u \\ v \end{pmatrix}$$

and use the matrix equation:

$$f = P(x_i - x^o{}_i)$$

where P is the 3 x 3N matrix of all weight coefficients and $(x_i - x^o{}_i)$ is a 3N vector corresponding to the measurements of the three basic variable at N different stations around the reference location.

The optimization criterion is now that the distance:

$$\overline{d^2} = t_r \, (f-f^o)(f_o-f)^T$$

be minimum and this is realized when:

$$P = (f-f^o)(f_i-f^o{}_i)^T \left[(f_i-f^o{}_i)(f_i-f^o{}_i)^T\right]^{-1} \qquad (9)$$

Provided enough <u>independent meteorological stations</u> could be used to establish stable values of the correlation coefficients which appear in expression (9), the matrix arithmetics are straightforward and yield appreciably better results than obtained by separate analyses of the three meteorological fields. Best results were found in this study when a damped persistence forecast was used as first guess, specifically:

$$f^o = \overline{f} + e^{-0.23t}(f^{-1} - \overline{f})$$

where f^{-1} is the result of the previous analysis at time -t

(days) and $\bar{f}$ is the climatological value. RMS errors for h, u, v were found: 14m, 4.1 m/sec and 3.4 m/s respectively when five stations at a mean distance of 400 km around Topeka, Kansas were used to provide estimates at this location. This is to be compared to 13 m, 4.0 m/sec and 3.4 m/sec respectively when 20 stations within a radius of 1000 km were used in the analysis and indicate that is does not pay to complicate the problem and to consider more than about five station surrounding the reference location.

Furthermore, analysis errors increased moderately when various groups of stations were used at increasing mean distances from the reference location vs:

Mean distance	h(m)	u($msec^{-1}$)	v($msec^{-1}$)
400km	14	4.1	3.4
600km	15	4.7	3.7
700km	16	5.1	4.4
800km	29	7.0	6.3

Finally, multivariate analyses are compared with the results of independent analyses of the geopotential height and wind fields, respectively, always using data from the five nearest stations.

Data used	h(m)	u($msec^{-1}$)	v($msec^{-1}$)
h,u,v	14	4.1	3.4
h only	18	4.8	4.3
u,v only	83	4.1	3.8

Time dependence of meteorological fields

Since meteorologists have been mostly interested in using synoptic data, all compiled at the same map time t, relatively little effort has been invested in establishing the covariance of meteorological variables in the time domain (equivalent information can be found in frequency power spectrum analyses performed with surface data, but not directly applicable to the problem at hand). The relatively good accuracy of 12 hours or one day forecasts based on persistence indicate that the correlation range of meteorological fields in the time domain certainly extends beyond one day. In fact, data available to this lecturer are consistent with a gaussian correlation range of two days. It is not known, however, how far deviations from a persistence forecast are correlated in the time domain. Additional work in thus certainly required here, particularly in view of the now pressing problem of analysis of non-synoptic data.

References

Gandin: Objective Analysis of Meteorological Fields (1963) Israel Program for Scientific Translations, Jerusalem, 1965 (242 p.).

Schlatter, T.W.: Some Experiments with a Multivariate Statistical Objective Analysis Scheme. Monthly Weather Review, 103, pp. 246-257 (1975)

8. Dynamic Response of the Large Scale Flow to Perturbations

Consideration of the mechanisms of energy conversion in large scale atmospheric circulation indicates that those motions which are able to transform consistently the thermal energy of the atmosphere into available potential energy should be such as to cross geopotential surfaces upward, and yet cross isentropic surfaces downward. The slopes of the corresponding air parcel trajectories must then be comparable to or less the slope of the isentropic surfaces.

Thus:

$$\frac{W}{U} \lesssim \frac{\left(\quad z\right)}{\left(\quad y\right)_{\theta}}$$

Now, the order of magnitude of the slope of isentropic surfaces can be inferred from the thermal wind equation which relates $\partial\theta/\partial y$ with the vertical wind shear.

$$\partial u/\partial z \approx U/D, \text{ and the known stability} \partial\theta/\partial z.$$

It turns out that

$$W \frac{D}{L} R_o \qquad (1)$$

where U is the characteristic velocity of the general atmospheric circulation D and L are the characteristic vertical and horizontal scales respectively, and Ro is the Rossby number. Under these circumstances, the scale analysis of the terms of the primitive dynamic equations for large scale atmospheric flow may proceed to yield eventually in the zero order of the (small) Rossby number:

$$\vec{fk} \times \vec{V} = -\alpha \nabla p \qquad (2)$$

$$\nabla \cdot \vec{V} = 0 \qquad (2a)$$

i.e. a stationery perfectly balanced geostrophic flow, while only in the first order of Ro we retrieve the familiar approximations of the continuity and vorticity equations which allow the propagation of Rossby waves :

$$\frac{d}{dt}\left(\text{curl}\, \vec{V} + f \right) + f_o \nabla . \vec{V} = o \qquad (3)$$

$$\frac{1}{\rho_s} \frac{\partial}{\partial z}(\rho_s W) + \nabla . \vec{V} = o \qquad (3a)$$

Thus the (non-dimensional) divergent wind must be of order Ro for large scale quasi-geostrophic flow obeying relation (1). On the other hand, the atmosphere could sustain much more violent vertical motions which do not however produce a net conversion of energy. These motions are gravity waves where the vertical velocity $W \sim UD/L$ and the associated divergent wind are at least one order of magnitude larger than those associated with quasi-geostrophic motions.

Why so little atmospheric kinetic energy is found in the gravity wave modes and so much in the quasi-geostrophic motions is not at all clear. The standard explanation of the dissipation of gravity waves is based on the argument that they are dispersive so that any initial wave packet spreads out at infinity. But since the Earth atmosphere is a finite rather than infinite medium, this argument is not completely convincing. The dissipation of gravity wave motions may be related to their 3-dimensional nature which allows the cascading of energy toward higher wave numbers and eventual dissipation by turbulence and molecular viscosity, while quasi 2-dimensional

geostrophic motions do not allow this cascade.
In any case, there must be one (or several) processes at work in the continuous atmospheric fluid which does or do not exist in truncated model flows with a finite number of degrees of freedom. And this has the effect of greatly enhancing the tendency of general circulation models to sustain strong gravity waves which must be damped by ad-hoc devices such as divergence dumping (suggested by R. Sadourny). This relates to our problem of letting one atmospheric circulation model relax toward a new (updated) balanced quasi-geostrophic state after the injection of external informations or measurements acquired from the real atmosphere.

The geostrophic adjustment problem

We shall consider for the sake of simplicity the case of an homogeneous fluid ($\rho = \rho_o$ = constant) with a free surface initially at rest on a rotating planet.
Let h, u and v be the three dynamic variables; height of the free surface, zonal and meridional component of the velocity, respectively. In the critical state $u = v = O$; $h = H$. The linearized dynamic and continuity equation for barotropic flow thus reads:

$$\frac{\partial u}{\partial t} = fv - g \frac{\partial h}{\partial x}$$

$$\frac{\partial v}{\partial t} = - fu - g \frac{\partial h}{\partial y} \qquad (4)$$

$$\frac{\partial h}{\partial t} = - H \left(\frac{\partial u}{\partial x} + \frac{\partial v}{\partial y} \right)$$

where u,v and (h-H) are first order perturbations. Expanding the perturbation velocity field in its rotational and divergent part, we get:

$$u = \frac{\partial \psi}{\partial y} + \frac{\partial \chi}{\partial x}$$
$$v = \frac{\partial \psi}{\partial x} + \frac{\partial \chi}{\partial y} \qquad (5)$$

in terms of a stream function ψ and a divergent wind potential χ. It is also convenient to consider a Fourier expansion of the three scalar fields ψ, χ and h such as :

$$\begin{pmatrix} \psi \\ \chi \\ h \end{pmatrix} = \exp.\ i(kx+ly) \begin{pmatrix} \psi_{kl}(t) \\ \chi_{kl}(t) \\ h_{kl}(t) \end{pmatrix}$$

Equations (5) now become for each Fourier component :

$$u = -\ il\psi + ik\chi$$
$$v = \quad ik\psi \quad il\chi$$

and equations (4) yield after a few rearrangements:

$$\frac{\partial \psi}{\partial t} = -\ f\chi$$
$$\frac{\partial \chi}{\partial t} = f\psi - gh \qquad (6)$$
$$\frac{\partial h}{\partial t} = H(k^2+l^2)\chi$$

Solutions of this system cannot lead to geostrophic adjustment in view of their purely oscillatory character. Indeed, a simple algebra yields the wave equation:

$$\frac{\partial^2 \chi}{\partial t^2} + \omega^2 \chi = 0$$

where :

$$\omega = \sqrt{f^2 + gH\,(k^2 + l^2)}$$

is the dispersion relation for gravity waves in shallow water. In order to obtain geostrophic adjustment, i.e. the evolution towards a quasi 2-dimensional quasi non-divergent geostrophic state, external gravity waves in this case (and both external and internal waves in the general case of a baroclinic atmosphere) must be filtered out by an appropriate damping process. The simplest approach to eliminate these motions with large vertical velocities and horizontal divergence is to add a viscous damping term acting on the divergent wind only, thus :

$$\begin{aligned} \frac{\partial \psi}{\partial t} &= - f\chi \\ \frac{\partial \chi}{\partial t} &= f\psi - gh - \nu\,(k^2+l^2)\chi \\ \frac{\partial h}{\partial t} &= H\,(l^2 + k^2\,)\chi \end{aligned} \qquad (7)$$

In any <u>stationary state</u> then; geostrophic balance is restored:

$$\begin{aligned} \chi_s &= o \\ f\psi_s &= gh_s \end{aligned} \qquad (8)$$

We notice now that both in their original form (6) or in their modified form (7) , the dynamic equations allow the exact conservation of one integral invariant :

$$\Omega = H(k^2 + l^2)\psi + fh \qquad (9)$$

Since:

$$\frac{\partial \Omega}{\partial t} = H\,(k^2+l^2)\,\frac{\partial \psi}{\partial t} + f\frac{\partial h}{\partial t} \equiv 0$$

Thus if a solution is found to equations (7), starting from any initial state ψ_o, χ_o, h_o, out of geostrophic balance, the integral invariant Ω will remain constant. The final (stationary) balanced state ψ_s, h_s, is reached after some unspecified history and verifies :

$$H(k^2+l^2)\psi_o + fh_o = H(k^2+l^2)\psi_s + fh_s$$
$$\equiv \left[H(k^2+l^2) + \frac{f^2}{g}\right]\psi_s$$

And finally :

$$\psi_s = x\psi_o + (1-x)\frac{gh_o}{f}$$

where

$$x = \frac{gH(k^2+l^2)}{gH(k^2+l^2) + f^2}$$

varies from x =0 when the characteristic dimensions of the perturbation are very large (k,l very small) to x = 1 for a small scale perturbation (k,l,very large). Introducing

the Rossby deformation radius :

$$\lambda^2 = gH/f^2$$

we can also write :

$$x = \frac{\lambda^2 (k^2 + l^2)}{\lambda^2 (k^2 + l^2) + 1}$$

Consequently we find that when the characteristic scale (or wavelength $2\pi \left[k^2 + l^2\right]^{-1/2}$) of the initial perturbation of the mass distribution h_o is much larger than the Rossby deformation radius, the final velocity field is adjusted to the mass field and geostrophically balanced :

$$x \approx 0$$

$$\psi_s \approx \frac{g}{f} h_o$$

$$\chi_s \approx 0$$

When, on the other hand, the characteristic scale is much smaller than the Rossby deformation radius, the final velocity is essentially the same as the initial(perturbed) velocity;

$$x \approx 1$$

$$\psi_s \approx \psi_o$$

$$\chi_s \approx 0$$

In the special case where the initial perturbation would be applied to the mass field only ($\psi_o = \chi_o = 0$) the fluid is still completely at rest in the final state ψ_s: there has been no assimilation whatsoever of the mass field perturbation and this perturbation has been dissipated entirely in the form of gravity waves. This fact has naturally great significance for the problem of updating or assimilation of external data into one consistent (balanced) state of motion of a dynamic model of the atmospheric flow.

References

J. Charney in Dynamic Meteorology,
Reidel Pub. Co. (1973)

W. Washington, Tellus, 16, pp. 530-534 (1964)

9. Meteorological Data Assimilation

PART I : Single Time-Level Methods

The advent of remote sensing of the atmospheric structure from orbiting satellites has raised the possibility that nearly continuous observations of atmospheric temperature on the global domain will be available. Aside from considerations of accuracy and representativeness, these space data differ from conventional data in two major aspects. First, the satellite derived meteorological data are dynamically incomplete in that only one meteorological variable (temperature) can be observed everywhere. Second, the observations are distributed in space and time, rather than at fixed locations and agreed synoptic times. It is thus quite appropriate to reconsider current operational practice for utilizing these mixed data in numerical weather prediction.

The function of data assimilation means, in the present context, any process whereby meteorological observations are absorbed into a numerical (truncated) representation of the atmosphere. A common numerical representation is a set of values of the dynamical parameters (u, v, T) defined at regularly spaced grid points. Assimilations may be distinguished from straightforward interpolation or "optimal objective analysis" by requiring that the resulting numerical representation be a complete description of the meteorological variables, governed by prescribed physical constraints such as model dynamic equations, and/or a variety of "balance" conditions. A perfectly assimilated state of an atmospheric model would be one in which the observations of the real atmosphere and the numerical

representation would be interchangeable and obey the relevant physical constraints; in practice, the degree of interchangeability is limited by errors of the observations and the prescribed model dynamics which define the constraints.

The multivariate objective analysis of geopotential height and wind on the 500 mb isobaric surface, as described in section 7 could rightly be considered a form of 2-dimensional analysis since the resulting assimilated state incorporates the 2-dimensional dynamic constraint of geostrophic balance at this level. Flattery's (1970) representation of atmospheric circulation in terms of 3-dimensional series of orthogonal functions may be considered a 3-dimensional assimilation on the ground that the functions used to represent atmospheric variability imply dynamic constraints. Similarly, a 4-dimensional representation of the meteorological variables should be such as to best fit all the observations distributed through the relevant space domain (global) and time domain (e.g. 24 hours interval). After this general introduction, we may now concentrate on methods which are rightly 3-dimensional and therefore take only into account diagnostic dynamic relations which constitute constraints applicable at one single time t when observations are introduced.

Diagnostic constraints are generally based on the assumption that any proper state of the atmosphere ought to be near to geostrophic balance and should remain so after the assimilation of new observations. The simplest such diagnostic relation is

the quasi-geostrophic divergence equation which results from applying the divergence operator $\nabla .$ to the quasi-geostrophic dynamic equation :

$$\left(\frac{\partial}{\partial t} + \vec{V}_\psi \cdot \nabla\right) \vec{V}_\psi + f\vec{k} \times \vec{V} + \nabla\phi = 0 \qquad (1)$$

$$\vec{V}_\psi = \vec{k} \times \nabla\psi \qquad (2)$$

Because the divergent wind is order 1 in Ro for quasi-geostrophic motion, this component of the velocity field does not appear in the tendency nor in the advection terms. Accordingly, the divergence equation is diagnostic at this order and reads :

$$\nabla . \left[(\vec{V}_\psi . \nabla)\ \vec{V}_\psi\right] - f\ \nabla^2\psi + \left[\vec{V} \times \nabla f\right] . \vec{k} + \nabla^2\phi = 0 \qquad (3)$$

Except for a small contribution of the divergent wind to the third term, this equation is expressed solely in terms of the streamfunction ψ of the non-divergent flow and the geopotential field ϕ . This relation, accurate to the first order of the Rossby number, thus replaces the zero order geostrophic relation :

$$-f\psi + \phi = 0 \qquad (4)$$

and has indeed been used to infer the wind field from the observed geopotential field on the same isobaric surface.

Another diagnostic relation may be inferred by specifying that the vertical velocity consistent with the mass and horizontal velocity fields be everywhere vanishingly small. This constraint is then a specialization of the ω -equation relating the vertical velocity to the mass field under condition of geostrophic balance. The ω -equation is most conveniently derived from the (quasi-geostrophic) vorticity equation:

$$(\frac{\partial}{\partial t} + \vec{V}_\psi \cdot \nabla)(\nabla^2\psi + f) + f_o \nabla \cdot \vec{V} = 0 \qquad (5)$$

and corresponding thermodynamic equation :

$$(\frac{\partial}{\partial t} + \vec{V}_\psi \cdot \nabla)\log\theta + \omega \frac{\partial}{\partial p} \log\theta_s = 0 \qquad (6)$$

where $\partial\theta_s/\partial p$ is the potential temperature stratification of the standard (mean) atmosphere. Equation is further simplified by using the approximate geostrophic relation (4) and the continuity equation :

$$(\frac{\partial}{\partial t} + \vec{V}_\psi \cdot \nabla)(\frac{1}{f_o}\nabla^2\phi + f) - f_o \frac{\partial \omega}{\partial p} = 0 \qquad (7)$$

Equation (6) on the other hand is more conveniently written in the form :

$$(\frac{\partial}{\partial t} + \vec{V}_\psi \cdot \nabla) \frac{\partial \phi}{\partial p} + \sigma_s \omega = 0 \qquad (8)$$

after using the standard expression of entropy :

$$\log\theta = \log\alpha + \frac{1}{\gamma} \log p \ ,$$

and the hydrostatic equation :

$$\frac{\partial \phi}{\partial p} + \alpha = 0$$

We have also introduced the coefficient σ_s to specify the standard atmospheric stratification :

$$\sigma_s = - \frac{\alpha_s}{\theta_s} \cdot \frac{\partial \theta_s}{\partial p}$$

Now, elimintating the mass field tendency $\partial \phi / \partial t$ from equations (7) and (8), one gets the geostrophic ω- equation:

$$(\nabla^2 + \frac{f_o^2}{\sigma_s} \frac{\partial^2}{\partial p^2}) \omega = - \frac{1}{\sigma_s} \nabla^2 \left[\vec{V}_\psi \cdot \nabla \left(\frac{\partial \phi}{\partial p} \right) \right]$$

$$+ \frac{f_o}{\sigma_s} \frac{\partial}{\partial p} \left[\vec{V}_\psi \cdot \nabla \left(\frac{1}{f_o} \nabla^2 \phi + f \right) \right] \qquad (9)$$

where only space derivatives of the geopotential field appear on the right-hand side. Note that for a wave-like perturbation (3-dimensional wavenumber k, ℓ, m), the left-hand side is proportional to the vertical velocity :

$$(\nabla^2 + \frac{f_o^2}{\sigma_s} \frac{\partial^2}{\partial p^2}) \omega \sim - (k^2 + \ell^2 + \frac{f_o^2 \, m^2}{\sigma_s}) \omega$$

The full ω - equation, unlike the continuity equation, provides an estimate of the vertical velocity field which does not depend on accurate observations of the horizontal velocity field. Thus specifying that ω be small everywhere yields a diagnostic equation :

$$-\nabla^2 \left[\vec{V}_\psi \cdot \nabla \left(\frac{\partial \phi}{\partial p} \right) \right] + f_o \frac{\partial}{\partial p} \left[\vec{V}_\psi \cdot \nabla (\nabla^2 \psi + f) \right] \approx 0 \qquad (10)$$

which has sometimes been proposed to relate the non-divergent wind field to the geopotential ϕ.

However simple (like (4)) or sophisticated (like (3) or (10)), diagnostic relations can only express an a-priori conception of the forecast model response to the initial perturbation or shock caused by the introduction of observed values of the dynamical parameters. They are only approximations of the true response yielded by the complex set of coupled algebraic relations which constitute a numerical scheme for integrating the primitive equations. Nor are they particularly accurate approximations of the very complicated instantaneous behavior of a real fluid at large Reynolds number, as demonstrated by laboratory experiments.

Thus, the use of a diagnostic relation may be considered as a (possibly) convenient first step in the process of meteorological data processing but could not be expected to provide a complete dynamical assimilation of the observations into one fully consistent state of the model atmosphere. For this reason, the use of the more sophisticated diagnostic equations, which may involve non-trivial mathematical difficulties, is progressively replaced by methods which make a direct use of the forecast model dynamics to test the correct "balance" of the assimilation. These methods which do not simply refer to one single instantaneous state but involve a continuous time sequence of the model flow, are generally known as 4-dimensional assimilation techniques.

10. Meteorological Data Assimilation

PART II : Four-dimensional Methods

Following McPherson (1975), four-dimensional data assimilation will be taken to mean a process which results in a consistent representation of the complete meteorological variables over some definite time interval, reflecting a mutual accommodation to observations distributed in space and time and governed by a set of time-dependent constraints subsequently referred to as the model dynamics. This definition is based on the properties of the resulting state or rather the resulting time sequence of states of motion of the model atmosphere, rather than the characteristics of the assimilation scheme itself. It does not suffice that the process of meteorological analysis involve several time levels to produce a consistent four-dimensional (optimal) assimilation of data distributed in time as well as in space. Indeed, the current practice almost always involve starting the analysis of new (synoptic) observations by updating a first guess which may be the previously analysed fields or a forecast based on the latest analysis, thereby introducing a memory of previous data. Four-dimensional assimilation on the other hand would consist in finding one historical sequence of model states consistent with the latest set of observations as well as all previous observations.

Methodology of 4-dimensional assimilation

Gandin and others have suggested extending the method of optimal interpolation in two dimensions (see section 6 above) to the full four-dimensional problem. This approach, which may be called statistical assimilation is of limited practicality at present because of the difficulty of determining complicated statistical correlations and incorporating non-linear, time-dependent constraints.

Another mathematically elegant approach, which has been pursued by Sasaki (1970) and others, consists in incorporating dynamical constraints in a variational treatment. However, the elegance of this variational assimilation method is overwhelmed by its difficulty when general constraints are introduced.

Thus most of the research has been centered around the less elegant but physically more tractable method of dynamic assimilation in which the numerical integration model serves as an integrator to provide consistency between the observation distributed in space and time. In this approach, a continuity integration of the model is interrupted whenever new observations become available and the current model state is updated by inserting the observed values in place of the computed values. This method which can be continued indefinitely also provides a ready mean to check how well the assimilation is going by comparing the running forecast with further observations as

they come along. Direct insertion of observed data refers to updating only the grid point value nearest to an observation; a preferable technique is interpolating the observations to several near grid points using the model computed values prior to insertion as a first guess (see section 7 above for optimal interpolation). In this context, insertion of new data may be done continuously, i.e. at the model time step nearest the time of the observation, or intermittently when a large enough batch of observations is available. A variety of numerical experiments have shown that both schemes are essentially equivalent.

Damping

Because the insertion of heterogeneous values of the meteorological fields (originating in the real atmosphere or some other external "reference" historical record) produces model unbalance and gravity oscillations, a scheme for damping these oscillations must be provided. A variety of damping schemes have been used,the most popular being based on the Euler-backward or Matsuno time stepping algorithm. Fig. 1 shows the amplification factor of this integration scheme for a periodic perturbation of frequency σ. Since the time step Δt must be chosen so that the scheme remains stable (amplification factor $\leqslant 1$) for all waves explicitely represented in the model, it will be clear that the Matsuno scheme is almost nearly neutral for large-scale meteorological motions associated with slowly evolving wavelike perturbations ($\sigma \Delta t \ll 1$) while rapidly travelling gravity waves ($\sigma \Delta t \sim 1$) are strongly damped. There is a lot to be said in favor of this convenient scheme but some reservations must also

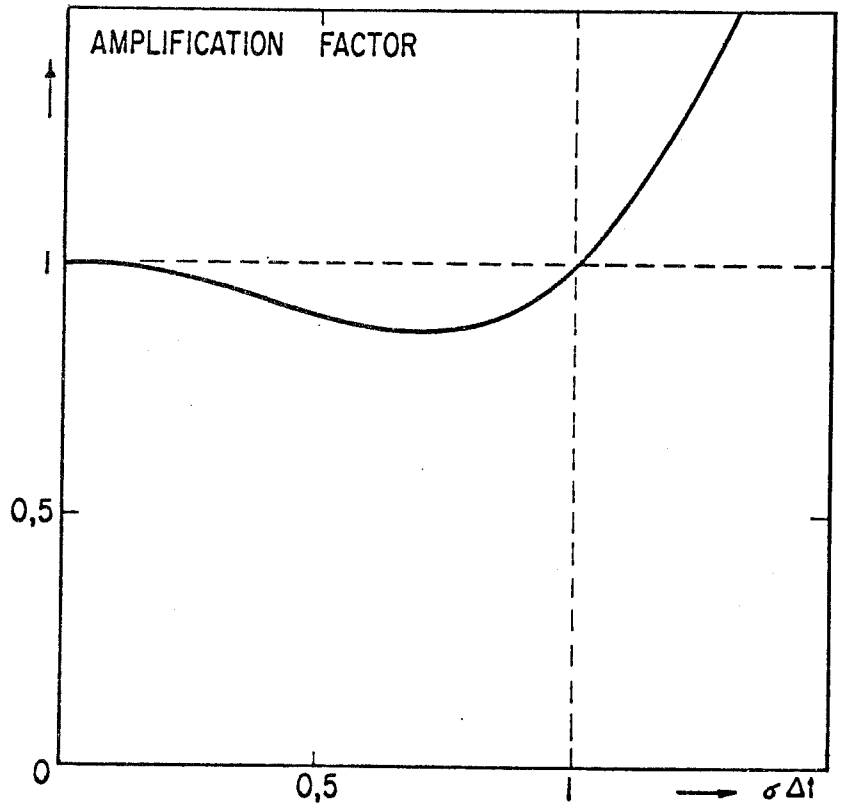

Fig. 1: (Ch.10)

Amplification factor of the Matsuno time integration scheme versus non-dimensional frequency $\sigma \Delta t$.

be made, the most serious of which is that long wavelength internal gravity modes associated with quite low time frequencies, are not damped at all. The same applies of course to so-called computational modes which have the shortest possible wavelength but are wrongly associated with frequency $\sigma = 0$ when the differential dynamic equations are approximated by space-centered finite difference equations.

Several authors have consequently preferred using a more selective if less convenient damping scheme which consists in adding an artificial viscosity term acting on the divergent part of the wind field only :

$$\frac{\partial \vec{V}}{\partial t} = - (\vec{V} \cdot \nabla) \vec{V} + \ldots + \kappa \nabla \cdot (\nabla \cdot \vec{V}) \qquad (1)$$

Here κ is an arbitrary artificial viscosity coefficient which may be adjusted to provide the most appropriate damping rate.

The dynamics of 4-dimensional assimilation

At the instant of insertion, the observations and the model representation of the flow are, by definition, interchangeable but they do not remain so. For example, if observations of the mass field are inserted into a primitive equation model without a perfect adjustment of the corresponding model representation of the wind field, an imbalance is created which is manifested by the development of gravity oscillations when the integration is resumed. This is referred to as the

initialization shock. It is obviously necessary (a) to minimize the initialization shock inasmuch as possible, e.g. by interpolating the observations to several nearby grid points instead of just inserting at one grid point, and (b) to damp out the gravity oscillations before new data are inserted and a new shock created. There is no way of inserting heterogeneous observations into a computed model state without creating gravity waves, unless an exact solution to the 3-dimensional assimilation problem were known. Thus damping these gravity oscillations is a necessary feature of any 4-dimensional assimilation scheme. Furthermore, not just any damping scheme is appropriate for the damping must be effective enough to prevent waves from building up and yet not so strong as to viciate the verisimilitude of the model and shorten the predictability range. In this context, it will be seen that inserting the same observation repeatedly in the course of the integration may have a detrimental effect through successive shocking of the model and the repeated production of gravity oscillations. In any case, the amount of damping is an adjustable parameter which must be optimized (empirically) to make one particular 4-dimensional assimilation procedure, applied with one particular general circulation model, converge best.

Next comes the matter of geostrophic adjustment already discussed in a previous lecture (see section 8 above). It has been found that a local change of the mass distribution, affecting a region much smaller than the Rossby deformation radius, does not yield a geostrophic adjustment of the wind field to the mass

field, but is simply dissipated in the form of gravity waves which propagate away and are eventually damped out. Thus a necessary condition for adjustment of the wind field is that pressure and temperature data be inserted regularly so as to fill large portions if not all of the spatial domain. But the mere existence of geostrophic adjustment (given an infinite time to respond to a perturbation of the mass field) does not tell us that the adjustment process is effective enough to operate in a practical situation where new observations and new shocks are introduced continuously. Thus we must also address the question of induction of the wind field by pressure and temperature observations only. In order to shed some theoretical light on the subject, let us call again on our model of an incompressible fluid of thickness H lying at rest on a rotating fluid.

Let us now introduce a perturbation h of the mass distribution by changing the height of the free surface according to some heterogeneous (external) observations without changing the velocity field. The question is to determine how these incomplete data could yield a complete representation of the meteorological variables. Let us recall then the dynamic equations for a wave-like perturbation :

$$\frac{\partial \psi}{\partial t} = - f\chi \qquad (2)$$

$$\frac{\partial \chi}{\partial t} = f\psi - gh - K(k^2 + \ell^2)\chi \qquad (3)$$

$$\frac{\partial h}{\partial t} = H(k^2 + \ell^2)\chi \qquad (4)$$

We can see now that the initial response of the wind field from its initial condition $\psi = \chi = 0$, will be governed by :

$$\frac{\partial \psi}{\partial t} \approx 0 \qquad (2a)$$

$$\frac{\partial \chi}{\partial t} \approx - gh \qquad (3a)$$

Thus, given a step function perturbation of the mass field, the response of the divergent part of the wind field will be linear while the response of the rotational wind will be initially parabolic and consequently much slower . We arrive then at this important conclusion that the divergent wind, directly coupled to the mass field through equations (3) and (4),reacts quickly. The rotational component is coupled only through the Coriolis term in equations (2) and (3); accordingly the major adjustment process needed to reconstruct the wind field is relatively slow and even extremely slow at low latitudes. One consequence of this dynamical property is that 4-dimensional assimilation cannot be based on the short term or differential response of the system only : one must allow enough time for the divergent wind response to develop.

Finally, we address the problem of rejection of observational information by the 4-dimensional assimilation process. Consider then a forecasting sequence leading to the forecast state A_o at time t_o when 4-dimensional assimilation of new observations begins. Let $A_o + \delta A_o$ the state reached after inserting the data available at time t_o. This new representation does not generally

coincide with a state of balance so that gravity oscillations are excited and eventually die out in the course of further integration (and appropriate damping) : Fig.2. At the end t_1 of the 4-dimensional assimilation time interval, balance is approximately restored but the balanced state so obtained is not consistent with the observations introduced at time t_o. Indeed, if the time integration was reversed to backtrack from t_1 to t_o, a third representation A_1 different from A_o and $A_o + \delta A_o$ would be reached. The reason is obviously that only a fraction of the available potential energy introduced at t_o could be used to induce the adjustment of the wind field, while the rest of the energy has been dissipated as damped gravitational oscillations. Accordingly, state A_1 incorporates only a fraction of the original updating corrections introduced at time t_o, the rest being rejected by the dynamics of adjustment. One single insertion and damping cycle cannot therefore yield a satisfactory assimilation. Assimilation obtains only if (a) the process is continued over several cycles provided the predictable period would extend over so many cycles or (b) the process is iterated many times over the same time interval (t_o, t_1) using the same data over again.

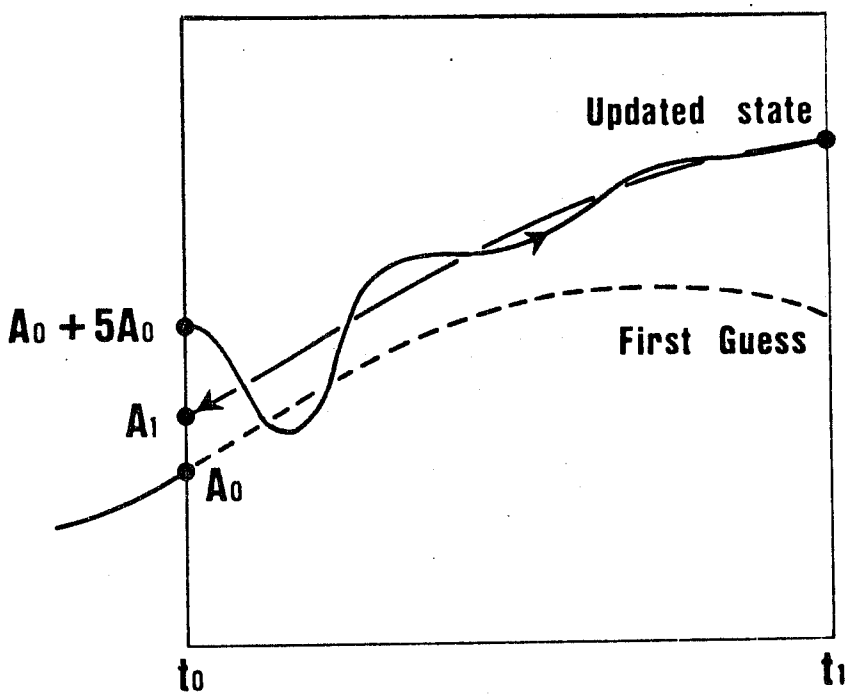

Fig. 2: (Ch.10)

Trajectory in phase space of a dynamical model of the atmospheric circulation after insertion of heterogeneous data at time t_o .

Numerical experiments in 4-dimensional assimilation

Many investigators have experimented with the various modifications of the basic 4-dimensional assimilation process described above, with a variety of artificially generated "reference" data or in some instances, real observations of the atmosphere. Although the quality of results did vary with the various improvements incorporated in the assimilation scheme, these operational differences are overshadowed by those resulting from the nature of the input data sets used in these experiments. Accordingly, three successive stages could be distinguished.

(i) The first experiment reported in the literature by Charney, Halem and Jastrow (1969) consisted in inserting directly temperature values in one particular "reference" historical sequence generated by one general circulation model, into a different run of the same model (started from an arbitrary initial state) and seing whether the velocity field could be so reconstructed from observations of the mass field only. This and similar experiments are cases of using a perfect model of the observed meteorological history, with infinite predictability : if one state of motion in the reference sequence could be reconstructed exactly then subsequent history would be predicted exactly. The results of the Charney, Halem and Jastrow study were very promising, indicating a quite accurate determination of the wind field even in the Tropics after about 15 days of continuous assimilation.

(ii) A second stage was almost immediately reached with a new set of experiments based on using artificial reference data generated by comprehensive general circulation models with "instrumental noise" added as random deviations, and again inserting these data in the same general circulation model considered now to provide forecasts of the reference history. Even though a perfect simulation of the reference system dynamics was still assumed in these experiments, the constant introduction of random noise did shorten the predictability period to 5 - 10 days (depending upon the RMS assumed errors) which correspondingly deteriorated results, specially at low latitudes (Fig. 3). The reason for the failure to reconstruct the wind field at low latitudes must be obvious to the reader : the shortened predictability period did not allow enough time for the slow adjustment of the non-divergent wind to proceed in the zone where $f \approx 0$. It is nevertheless on the basis of these imperfect experiments that the current plans for the First GARP Global Experiment could be established.

(iii) Finally, the third and final stage is now reached where 4-dimensional assimilation experiments are conducted with real observations or "realistic" artificial data generated by a different general circulation model so as to include the effect of <u>imperfect simulation</u> of the reference system dynamics. Fig.4 shows the result of one such experiments run at N.C.A.R. with two versions of the same basic model with 5° spatial resolution and 2.5° spatial resolution respectively. Although the

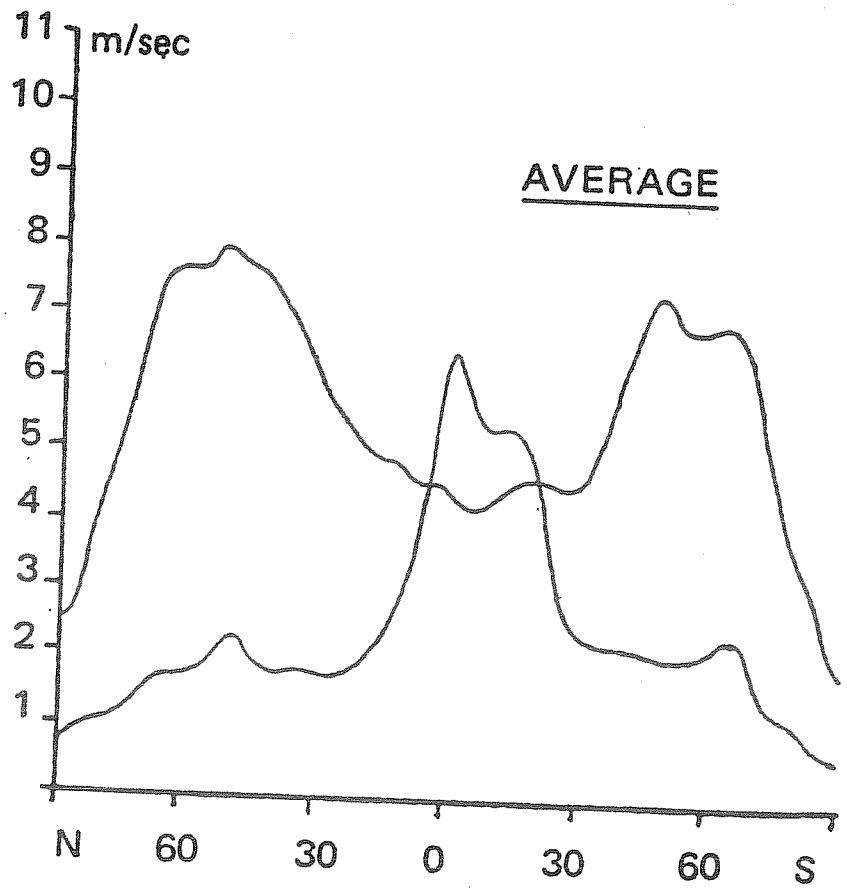

Fig. 3: (Ch.10)

Typical residual RMS error of the reconstructed wind field, compared to the reference data variability. Reference temperature data are generated by the same general circulation model with random errors added, (courtesy Geophysical Fluid Dynamics Lab., Princeton N.J.).

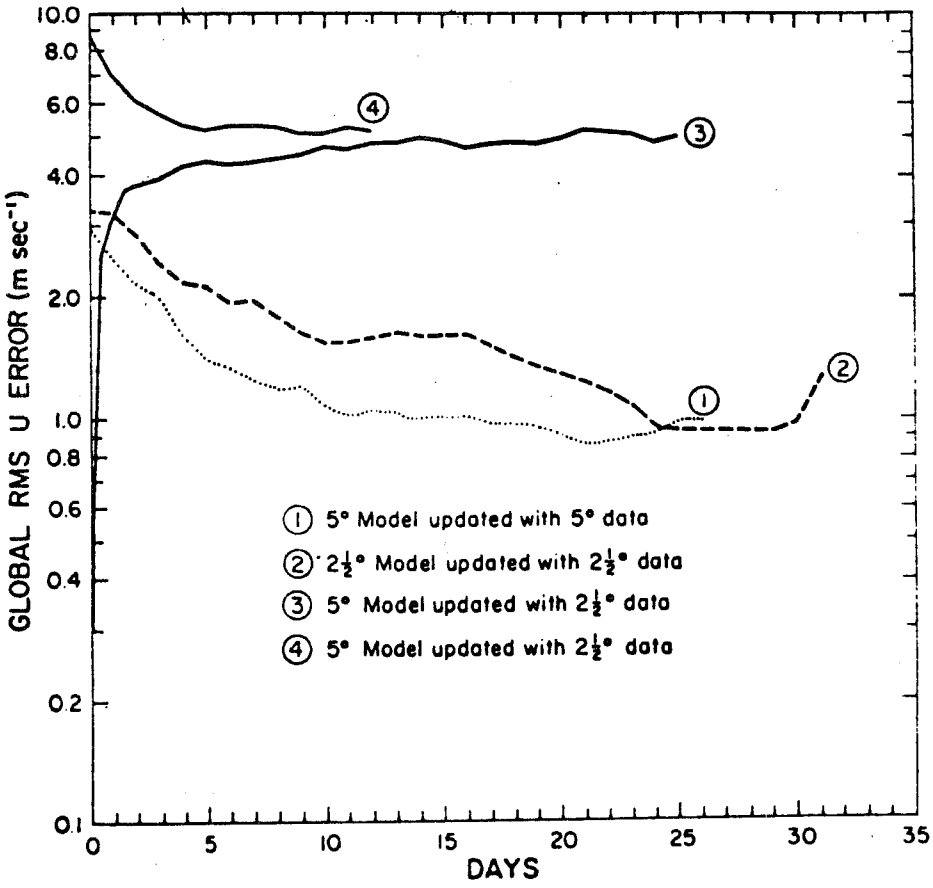

Fig.4: (Ch.10)

Assimilation experiments with artificial data generated by the same general circulation model (1,2) or a different model (3,4) (from Williamson, Tellus, 16, 530-534, 1964).

assimilation of 5° pressure and temperature data by the 5° model, or 2.5° data by the 2.5° model proceeded very well and yielded essentially the same (small) residual velocity error of 1 m sec^{-1} (RMS), the assimilation of 2.5° data by the coarser 5° model produced a much larger error of about 6 m sec^{-1} (RMS). The reason for this drastic deterioration is that the much shortened predictability of the 2.5° model by the 5° model reduced very much the adjustment of the non-divergent quasi-geostrophic wind field.

We conclude thus that if the insertion of pressure and temperature data is to induce an adjustment of the (rotational) wind field, this process must be fast so that assimilation could proceed far enough before the growth of forecast errors causes an overwhelming divergence. In this perspective, any procedure which could speed up the adjustment of the rotational wind also improves the accuracy of the reconstruction, as demonstrated by Kistler and McPherson (1975) in a series of experiments in which the local geostrophic wind values were inserted in addition to the geopotential height data (Fig.5).

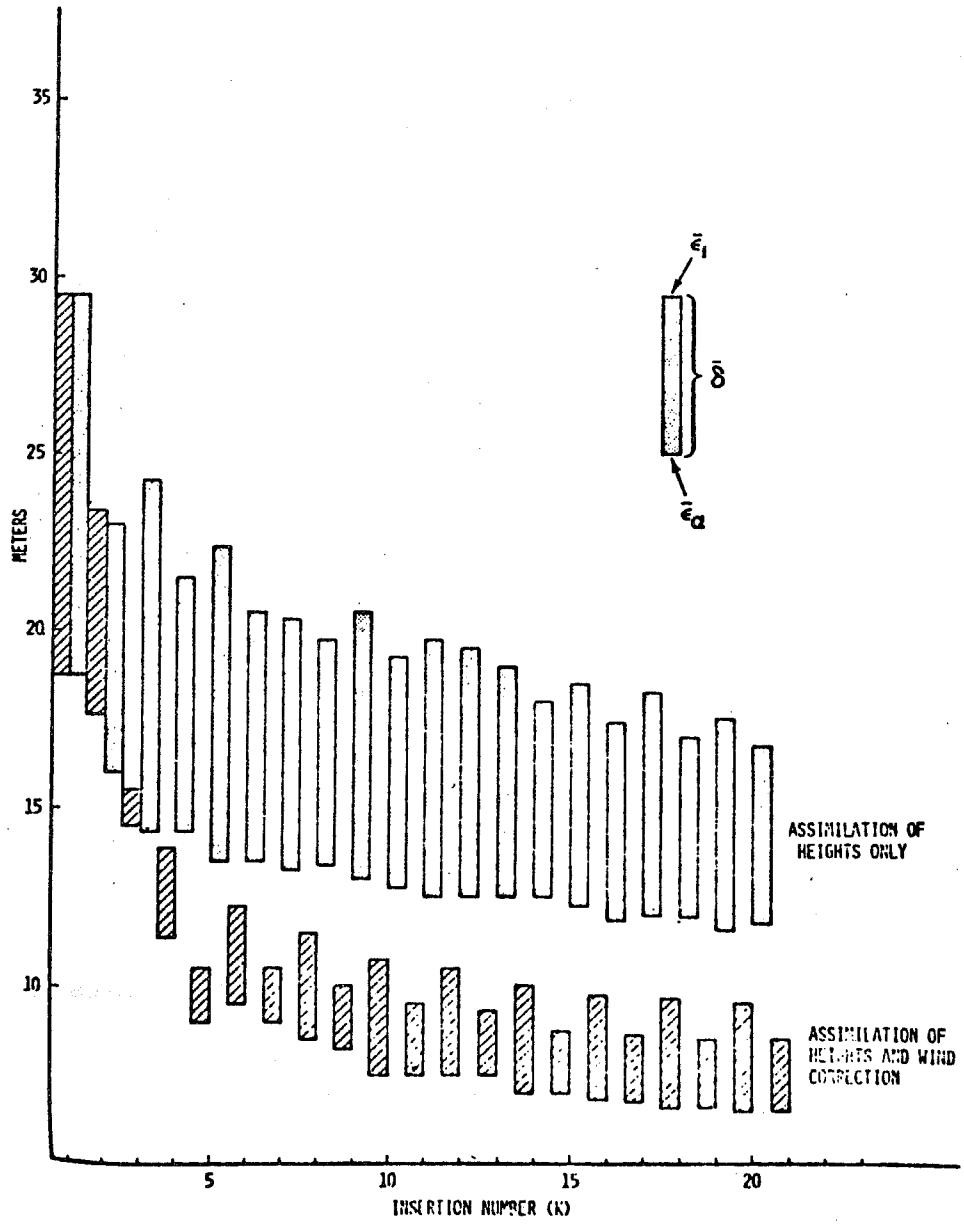

Fig. 5: (Ch.10)

Compared residual errors of the reconstructed wind field using geopotential data only (upper curve) or geopotential plus the local geostrophic wind value (lower curve) , (from Kistler and McPherson,op.cit.).

REFERENCES

1 - CHARNEY, HALEM and JASTROW : Use of incomplete historical data to infer the present state of the atmosphere. J. Atmos. Sci., 26, 1160-1163, 1969.

2 - KISTLER and McPHERSON : On the use of a local wind correction technique in four-dimensional data assimilation. Monthly Weather Rev., 103, 445-449, 1975.

3 - McPHERSON : Progress, Problems and Prospects in Meteorological Data Assimilation, N.M.C., Office Note 110, NOAA, Washington D.C. (1975).

For more information on this topic, see also BENGTSSON : Four-dimensional assimilation of meteorological observations. GARP Publication Series n°15 (1974).